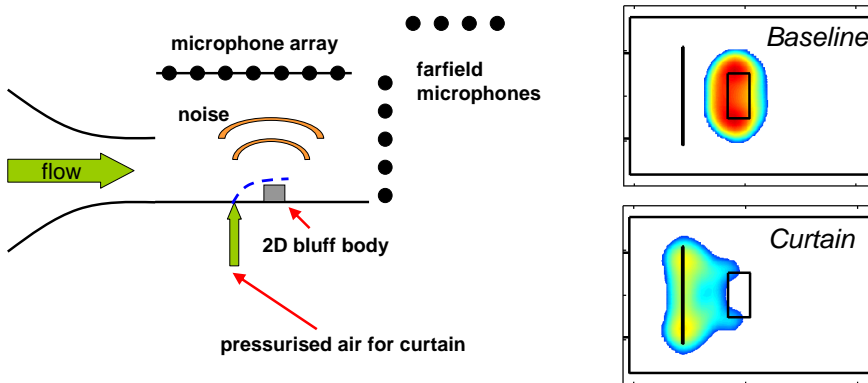




## Executive summary

# Reduction of Landing Gear Noise Using an Air Curtain



### Problem area

For modern aircraft, landing gears are the dominant noise source during approach and landing. In order to reduce noise hindrance and enable further growth of air traffic, noise reduction means are desired.

### Description of work

Small-scale proof-of-concept tests were performed in NLR's Small Anechoic Wind Tunnel on an air-curtain. The idea of this concept is to apply an upstream blowing slot to deflect the flow around a landing gear component, thus reducing the local flow speeds and therefore the aerodynamically generated noise. Two-dimensional half-models were mounted on an endplate which was attached to the lower edge of the nozzle. Blowing was applied through a slot in the endplate, upstream of the model. Microphone array and PIV measurements were

performed to characterize the acoustics and aerodynamics of the air curtain. Tests were done for different wind tunnel speeds, blowing speeds, slot geometries and model geometries.

### Results and conclusions

For the relatively quiet baseline half-models in the present tests, broadband noise reductions of 3-5 dB were obtained using an air curtain with vertical blowing. The noise reductions could be increased by oblique blowing and by applying a small flow deflector directly behind the blowing slot. For full models larger noise reductions are anticipated.

### Applicability

The air curtain technology is a promising concept for the reduction of landing gear noise.

### Report no.

NLR-TP-2009-403

### Author(s)

S. Oerlemans  
A.C. de Bruin

### Report classification

UNCLASSIFIED

### Date

August 2009

### Knowledge area(s)

Aëro-akoestisch en experimenteel  
aërodynamisch onderzoek

### Descriptor(s)

landing gear  
airframe noise





NLR-TP-2009-403

## Reduction of Landing Gear Noise Using an Air Curtain

S. Oerlemans and A.C. de Bruin




This report is based on a presentation held at the 15th AIAA/CEAS Aeroacoustics Conference, Miami, Florida, 11-13 May 2009.

The contents of this report may be cited on condition that full credit is given to NLR and the authors.

This publication has been refereed by the Advisory Committee AEROSPACE VEHICLES.

Customer                      European Commission  
Contract number              ----  
Owner                            NLR  
Division NLR                   Aerospace Vehicles  
Distribution                    Unlimited  
Classification of title        Unclassified  
October 2009

Approved by:

Author	Reviewer	Managing department
 19/10/09	 19/10/09	 27/10



## Contents

<b>I</b>	<b>Introduction</b>	<b>5</b>
<b>II</b>	<b>Design study</b>	<b>5</b>
	A Aerodynamic considerations	6
	B Acoustic considerations	7
	C Test objectives	8
<b>III</b>	<b>Test set-up</b>	<b>9</b>
	A Wind tunnel	9
	B Blowing system	9
	C Models	9
	D PIV measurements	10
	E Acoustic measurements	10
	F Test program	11
<b>IV</b>	<b>Results and discussion</b>	<b>11</b>
	A Planar jets without cross-flow	11
	B Planar jets in cross-flow	12
	C Noise reduction potential	13
<b>V</b>	<b>Conclusion</b>	<b>14</b>
	<b>References</b>	<b>15</b>



This page is intentionally left blank.

# Reduction of Landing Gear Noise Using an Air Curtain

Stefan Oerlemans<sup>1</sup> and Anton de Bruin<sup>2</sup>

National Aerospace Laboratory NLR, 8300 AD Emmeloord, The Netherlands

Acoustic and aerodynamic measurements were performed in NLR's Small Anechoic Wind Tunnel on the air curtain concept, which is intended for landing gear noise reduction. The idea of this concept is to apply an upstream blowing slot to deflect the flow around a landing gear (component), thus reducing the local flow speeds and therefore the aerodynamically generated noise. Prior to the wind tunnel tests, a design study was carried out to assess the possible benefit of an air curtain and to define the test set-up. For the subsequent proof-of-concepts tests, two-dimensional half-models were mounted on an endplate which was attached to the lower edge of the wind tunnel nozzle. Blowing was applied through a slot in the endplate, upstream of the model. Microphone array and PIV measurements were performed to characterize the acoustics and aerodynamics of the air curtain. Tests were done for different wind tunnel speeds, blowing speeds, slot geometries and model geometries. For the relatively quiet baseline half-models in the present tests, broadband noise reductions of 3-5 dB were obtained using an air curtain with normal blowing (i.e. perpendicular to the main flow). The noise reductions could be increased to 5-10 dB by oblique blowing (30° upstream) or by applying a small flow deflector directly before the blowing slot. For full models larger noise reductions are anticipated.

## I. Introduction

FOR modern aircraft, landing gears are important noise sources during approach and landing. In order to alleviate noise hindrance and enable further growth of air traffic, noise reduction means are desired. The amalgam of landing gear parts, each interacting with and exposed to the wakes of other parts, produces broadband noise. Streamlining of these components is not an easy task because of their complexity and/or functionality. Therefore, within the European TIMPAN project (Technologies to Improve Airframe Noise), several innovative methods for reducing landing gear noise are investigated.

The present study considers the air curtain concept, which is intended for landing gear noise reduction. The idea of this concept is to apply an upstream blowing slot to deflect the flow around a landing gear (component), thus reducing the local flow speeds and therefore the aerodynamically generated noise. Since broadband landing gear noise typically scales with the 6<sup>th</sup> power of the local flow speed, in principle significant noise reductions can be obtained. Key question is whether the noise reduction at the obstacle is large enough to compensate for the additional noise created by the air-curtain itself. Also there may be detrimental effects because of an interaction between the (unsteady) jet flow and the bluff-body structure. The goal of the present study is to obtain a *proof-of-concept*; the implementation in a complete aircraft system will be evaluated at a later stage in the project.

In this paper, first a design study is carried out, in which the potential benefit of an air curtain device is assessed on the basis of previous aerodynamic and aeroacoustic investigations into planar jets (Section II). Next, the concept is experimentally assessed through acoustic and aerodynamic measurements in a small anechoic wind tunnel. The test set-up is described in Section III, and the experimental results are discussed in Section IV. The conclusions of this study are summarized in Section V.

## II. Design study

The local flow speeds at landing gear components can be reduced in several ways by blowing. One possibility is presented in Figure 1, which shows a double-slotted air curtain device for deflecting the flow around a bluff body obstacle. Two-sided lateral blowing (i.e. perpendicular to the main flow) is applied from a strut upstream of the obstacle in order to deflect the flow, similar to a large streamline cap. Possible advantages of the blowing slot device

<sup>1</sup> Senior scientist aeroacoustics, P.O. Box 153.

<sup>2</sup> Senior scientist aerodynamics, P.O. Box 153.

with respect to a streamline cap are its smaller size and the fact that it leaves critical shielded parts accessible for visual inspection. For the present proof-of-concept study, we will leave aside the question of how such a small blowing device can be constructed, and focus on an assessment of the potential acoustic benefit of the air-curtain device. Such an assessment can be well made using the half-model implementation sketched in Figure 2, where the air curtain device can be kept outside the flow, and there is no need to develop a small device. This implementation may also represent a configuration where the blowing device is located inside the fuselage of an aircraft, and the air curtain shields (part of) the landing gear. Because of its practical advantages, the half-model set-up is chosen for the experiments, and will therefore also be considered in this section. In the following sub-sections we will discuss the aerodynamic aspects of an air curtain, the acoustic aspects, and the resulting test objectives. Although this design study focuses on normal blowing (perpendicular to the main flow), we will also shortly discuss the aerodynamic effects of oblique blowing and a flow deflector just upstream of the blowing slot, since these concepts are also tested during the experiments. The relations derived in this section will be assessed against the experimental results in Section IV.

### A. Aerodynamic considerations

Experimental results and theory on planar turbulent jets issuing *in still air* are for example given in Ref. [1]. With  $x$  the distance to the nozzle along the centerline, the velocity in a planar jet developing in still ambient conditions decays as  $x^{-1/2}$ , and its half-width  $b_{1/2}$  is roughly proportional to  $x$  as:  $b_{1/2} = 0.11x$ . Planar jets *in cross-flow* are mainly used to block flows through channels or at entrances. The planar jet is then blowing at an oblique angle against the oncoming flow (usually about  $30^\circ$  with respect to flow-normal direction), in order to create an over-pressure that blocks the channel flow. This latter application is usually referred to as the air-curtain technique [2,3].

A planar (turbulent) jet, blowing through a slot normal to the oncoming flow, can also be used to create a local stagnation line in the flow in order to deflect the main flow. This leads to a recirculation region with relatively low velocities behind it. The aerodynamic characteristics of planar jets in cross-flow were considered in Refs. [4,5]. A schematic view of the flow is given in Figure 3. For a cross-flow velocity  $V$  and a jet velocity  $V_j$ , the velocity ratio is defined as  $R = V_j/V$ . The width of the blowing slot is indicated by  $h$ . Introducing a momentum length scale  $l_m = hR^2$ , Ref. [4] gives the following relation for the jet centerline position:

$$x/l_m = c_j (y/l_m)^{1/2}, \quad (2.1)$$

where  $x$  is the height,  $y$  is the streamwise distance behind the slot (Figure 3), and  $c_j$  is a proportionality constant, for which a value of 1.2 was found. This relation can be converted to:

$$x = c_j R \sqrt{hy}. \quad (2.2)$$

Because of the jet spreading rate, the effective shielding height starts to decrease at a certain downstream position. According to Ref. [4] the spreading rate of jets in cross-flow tends to be larger than the spreading rate of jets without cross flow, especially at later stages. Based on their results the jet half-width can be estimated by

$$b_{1/2} \approx c_b s, \quad (2.3)$$

with  $s$  the distance along the (curved) jet centerline and  $c_b$  a proportionality constant with a value between 0.12 and 0.15. We can use Eqs. (2.2) and (2.3) to determine the target centerline position  $(y_t, x_t)$  corresponding to the maximum effective shielding height  $x_e$ , by demanding  $dx/dy = c_b$ . Using a conservative estimate of  $c_b = 0.15$  (large spreading), it turns out that

$$y_t = 16hR^2; \quad x_t = 4.8hR^2; \quad x_e = 1.9hR^2, \quad (2.4)$$

which shows that due to the jet spreading, the effective shielding height is only about 40% of the centerline height. The optimum streamwise distance behind the slot is found to be about 8 times the effective shielding height.





Moreover, the maximum shielding height is found to be proportional to the slot width and the square of the velocity ratio.

It should be noted that the above estimates are based on engineering approximations. Nevertheless we can use them to get an idea of the required jet noise velocity and mass flow for a given shielding height in the half-model wind tunnel set-up. Figure 4 shows the required jet velocity as a function of slot width, for different effective shielding heights. It can be seen, for example, that for a shielding height of 50 mm, the required velocity ratio is 3.6 for a 2-mm slot, and only 1.5 for a 12-mm slot. The corresponding mass flows, assuming a slot length of 44 cm and a cross-flow of 70 m/s (as in the subsequent wind tunnel tests), are given in Figure 5. This figure shows that the required mass flow is lowest for a small slot width. However, due to the higher jet velocities, the noise production will probably be higher. This will be investigated in Section IIB.

Besides the normal blowing concept depicted in Figure 2, the effects of 30° upstream blowing (Figure 6) and a flow deflector just upstream of the blowing slot (Figure 7) are also investigated in the experiments. In the following we will try to estimate the effect of these two concepts. The action of a deflector with height  $d$  is two-fold: (1) it deflects the flow upstream of the deflector away from the wall (creating additional vertical impulse), and (2) it causes the jet to start effectively at height  $d$ . Based on these experimental observations (see Section IVB) a revised model for the jet trajectory is postulated, based on a modified momentum length scale  $l_m$ :

$$l_m = (c_v d V^2 + h V_j^2) / V^2 = c_v d + h R^2. \quad (2.5)$$

In this equation, the model parameter  $c_v$  is an empirical constant ( $c_v < 1$ ) to account for the vertical impulse induced by the air scooped by the deflector. Assuming that the jet trajectory starting at the top of the deflector is still described by Eq. (2.1), the modified trajectory height for the case with deflector becomes:

$$x = d + c_j \sqrt{y} \sqrt{c_v d + h R^2}. \quad (2.6)$$

For the oblique blowing slot the jet height is found to increase with respect to normal blowing (see Section IVB). We suppose that the oblique jet trajectory is described by a parabola, as in Eq. (2.2), but that the top of that parabola lies  $\Delta x$  above and  $\Delta y$  upstream of the blowing slot. With the shape of the parabola described by Eq. (2.2), the point where  $dx/dy = \tan 30^\circ = \sqrt{3}$  defines these distances. Evaluation gives:

$$\Delta x = c_j^2 R^2 h / 2\sqrt{3} \quad \text{and} \quad \Delta y = \Delta x \sqrt{3} / 6. \quad (2.7)$$

Assume now that the first part of the jet (up to height  $\Delta x$ ) represents an extra obstruction to the oncoming flow, similar to a flow deflector having height  $d = \Delta x$ . Substitution in Eq. (2.6) then gives the following trajectory for the oblique blowing jet:

$$x = \Delta x + c_j \sqrt{y + \Delta y} \sqrt{c_v \Delta x + h R^2}. \quad (2.8)$$

Note that, contrary to the case with a fixed deflector height, the obstruction height  $\Delta x$  now progressively increases with  $R$ . The above equations will be assessed against the experimental results in Section IVB.

## B. Acoustic considerations

Information on jet noise is mainly available for circular jets. Much less information is available for jets from high aspect ratio nozzles. No information could be found on the effect of cross-flow on the noise production of planar jets. Information on planar subsonic jets in relation to other jets is given in Refs. [6,7].

Aeroacoustic experiments with high aspect ratio planar jets (without cross-flow) were reported by Munro and Ahuja [8,9]. Rectangular jets with widths  $h$  between 0.66 and 1.45 mm and lengths  $w$  between 17 and 76 cm were tested, leading to jet aspect ratios between 100 and 3000 (12 different cases). The noise was measured at different observation angles  $\theta$  to the downstream jet axis, at a distance  $R_m$  of 10 ft (3.048 m) and for jet speeds  $V_j$  between 150 and 335 m/s. Their study included a thorough analysis on the relevant scaling parameters for overall sound



levels and noise spectra of planar jets in relation to that of circular jets. They found the following scaling for the noise level from high aspect ratio nozzles:

$$p^2 \sim \frac{\rho_m^2 V_j^8 L_{eq}^2}{\rho_0 a_0^5 R_m^2} (1 - M_c \cos \theta)^{-5}, \quad (2.9)$$

where  $p$  is the acoustic pressure,  $\rho_0$  is the ambient mean density,  $\rho_m$  is the density in the mixing region,  $a_0$  is the ambient speed of sound,  $L_{eq}$  is an equivalent length scale, and  $M_c$  is the convective Mach number. Based on the experimental results the convective Mach number was approximated as  $M_c = 0.36M_j$ , and the equivalent length scale was defined as:

$$L_{eq} = h^{3/4} w^{1/4}. \quad (2.10)$$

Note that for an observation angle  $\theta$  of  $90^\circ$  the convective Mach number plays no role. By normalizing the spectral levels according to Eq. (2.9), and plotting them versus the normalized frequency

$$f^+ = \log \left[ f L_{eq} (1 - M_c \cos \theta) / V_j \right], \quad (2.11)$$

Munro and Ahuja [8] were able to collapse all measured spectra at a given observer angle within about 5 dB. Their normalized spectra for  $\theta = 90^\circ$  are shown in Figure 8, where the green solid line indicates the approximated generic spectrum that will be used subsequently in the present study. A different generic spectrum was found for  $\theta = 20^\circ$ .

We can use Eqs. (2.9) to (2.11) in combination with Figure 8 to estimate the noise from the normal jets considered in the previous section (neglecting possible effects of cross-flow on the jet noise). With  $SPL_{norm}$  and  $f_{norm}$  the normalized level and frequency as read from Figure 8, and all other variables in metric units, the dimensional sound level  $SPL$  and frequency  $f$  are determined by

$$\begin{aligned} SPL_{norm} &= SPL + 20 \log(R_m) - 10 \xi \log(V_j) - 20 \log(h^\gamma w^{1-\gamma}) + 50 \log(1 - M_c \cos \theta) + 98.72 \\ f_{norm} &= \log \left[ f h^\gamma w^{1-\gamma} (1 - M_c \cos \theta) / V_j \right] \end{aligned} \quad (2.12)$$

where  $\xi = 8$  and  $\gamma = 0.75$  (these parameters will be varied in the analysis of the experimental results). Note that  $\gamma$  is *not* the ratio of the specific heats  $c_p/c_v$ . The estimated peak level for the previously discussed normal jets as a function of slot width and shielding height is presented in Figure 9. This figure shows that for a given shielding height the noise from the jet decreases for increasing slot width, as a result of the lower jet velocity (Figure 4). However, as mentioned before (Figure 5), the larger slot widths require larger mass flows. Thus, in practice a compromise must be found between the mass flow requirement and the jet noise production.

In order to assess the potential for noise reduction, the generic spectrum from Figure 8 is used to estimate the spectrum of an air curtain with a shielding height of 5 cm. In Figure 10 the estimated spectra for three slot widths are compared to the measured spectrum of a 2D strut with a 5-cm H-shaped cross section, that was tested before in the same wind tunnel at 70 m/s wind speed (sound levels are normalized to the same distance). The measured background noise spectrum is plotted as well. It can be seen that, if we neglect possible excess noise due to interaction between the air curtain and the strut, it is in principle possible to obtain a substantial noise reduction using a normally blowing air curtain device. As expected on the basis of Figure 9, the estimated noise levels decrease with increasing slot width, due to the lower blowing speeds (see Figure 4).

### C. Test objectives

It should be noted again that many approximations have been made in the above estimations, such as neglecting the effect of cross-flow on the jet noise level and directivity, and neglecting possible excess noise due to interaction between the curtain and the strut. Therefore the actual noise reduction potential of the air curtain concept has to be determined in the wind tunnel tests. Thus, the objectives of the test campaign are (1) to measure the aerodynamic



and aeroacoustic characteristics of the air curtain as a function of  $V$ ,  $V_j$ , and  $h$ , (2) to compare the experimental results to the above estimations on the basis of literature, and (3) to determine the noise reduction potential of an air curtain in combination with a generic bluff body. Besides  $V$ ,  $V_j$ , and  $h$ , we will also vary the shape and height of the bluff body, the distance between the blowing slot and the bluff body, and we will investigate the effects of oblique blowing or a flow deflector just upstream of the blowing slot.

### III. Test set-up

#### A. Wind tunnel

The measurements were performed in NLR's Small Anechoic Wind Tunnel KAT (Figure 11). The KAT is an open circuit wind tunnel, the test section of which is surrounded by a  $5 \times 5 \times 3 \text{ m}^3$  room which is completely covered with 0.5 m foam wedges, yielding more than 99% absorption above 500 Hz. Two-dimensional half-models were mounted on an acoustically lined endplate which was attached to the lower edge of the  $0.5 \times 0.4 \text{ m}^2$  nozzle. The lined endplate consisted of a 5.5 cm layer of sound absorbing foam which was covered by a 5% open perforated plate, and was integrated with the blowing system. Blowing was applied through a 436-mm slot in the endplate, upstream of the model (Figure 6). For normal blowing, tests were made with 4-, 8- and 11-mm slot widths, for oblique blowing ( $30^\circ$  upstream) the slot width was fixed to 8 mm. Verification measurements showed that the smallest slot actually had a width of 3.8 mm, instead of the intended 4 mm. Therefore, in the analysis of the results a value of 3.8 mm is used, although for conciseness the slot will be denoted as the '4-mm slot'. During some tests a 25-mm quarter-circle flow deflecting element (Figure 7) was placed just in front of the blowing slot, in order to create a larger shielding height for a given jet velocity. This configuration proved successful and therefore also alternative 25- and 10-mm non-streamlined L-shaped deflectors were tested. The effect of inflow turbulence could be assessed by mounting a turbulence grid in the wind tunnel nozzle.

#### B. Blowing system

Pressurized air was introduced in the settling chamber through two  $\frac{3}{4}$ -inch hoses on both lateral sides at the bottom of a 400-mm diameter round vessel type settling chamber (Figure 12). A number of measures were taken to prevent extraneous noise from the pressurized air supply radiating from the blowing slot, such as damping material inside the last part of the two connection hoses, foam inside the large vessel, and a 'sandwich' of foam layers in the upper rectangular part of the settling chamber. In this way it was ensured that possible extraneous noise due to the air supply was suppressed.

The mass-flow through the slots was regulated by a sonic venturi. The front and back pressure of the sonic venturi, the air temperature and the metal temperature of the sonic venturi itself were measured and together yielded the calibrated mass-flow rate. For the present tests mass flow rates of up to 0.7 kg/s were used. With the given cross-sectional area of the blowing slot and the measured air temperature in the plenum chamber of the blowing slot device, the mean jet velocity was defined within 1%. In order to verify the two-dimensionality of the slot flow, and to check the jet velocity and mass-flow through the slot, measurements were done with a 3-mm pitot-static tube with its tip about 5 mm above the 4 mm slot exit. Measurements were done at the middle of the slot and at 100 and 200 mm aside from the middle of the slot.

#### C. Models

One of the goals of the test was to assess the performance of the air curtain with a half-model which is representative for a landing gear component. The most important requirement for the model was that it produced sufficient broadband noise and no extraneous noise sources. For this purpose, two rectangular half-models were selected to represent generic landing gear components. The height of the models was 25 and 50 mm, and the width was 50 and 100 mm respectively (so that the full models would have a square cross-section). Initially the model length was equal to the width of the endplate, i.e. 700 mm (Figure 6). However, during the first tests with the rectangular models in combination with an air curtain, extraneous noise sources were observed at the model edges. These sources may have been caused by (1) interaction between the tunnel shear layer and the model edges, (2) 3D flow from the slot corners [10] interacting with the model, and/or (3) stagnating flow in front of the model pushing the flow sideways. This motivated the use of two shorter rectangular models, with the same cross section but with a length of only 200 mm, so that the complete model was inside the tunnel flow and extraneous edge sources were prevented. These results suggest that in practical applications the blowing slot should be longer than the component to be shielded. It should be noted that the relative importance of these edge effects becomes smaller as the component length increases. All results presented in this paper are for the shorter models.

#### D. PIV measurements

Particle Image Velocimetry measurements were done to characterize the air curtain flow. Seeding with about 1 micron sized Di-Ethyl-Hexyl Sebacate (DEHS) particles was provided by a seeding generator. The flow particles were led to six 4-mm diameter holes on each side of the rectangular upper part of the plenum chamber of the blowing device, in the immediate neighborhood of the slot symmetry plane (Figure 12). The particles then convected through the slot exit of the air curtain.

A double pulse Nd:YAG – laser with 2 x 230 mJ was positioned outside of the KAT test chamber. Laser light was transmitted through a Laser Light Guide (an articulated arm) to a cylindrical lens mounted above the nozzle of the KAT wind tunnel (Figure 11) in order to illuminate the wind tunnel symmetry plane in the region starting from just in front of the blowing slot until about 35 cm downstream. The test area was observed from aside with a PCO double-shutter, 1.3 Megapixel (1280 x 1024 pixel) camera, allowing measurement of the two velocity components in the tunnel symmetry plane, in the region around the blowing slot up to the downstream model position. Each PIV measurement actually consisted of 100 double exposure PIV image sets, gathered with an acquisition rate of 3.33 Hz. The time difference between the two images varied between 10 to 50  $\mu$ s to get optimum results depending on the jet and tunnel velocity.

Example PIV seeding intensity maps are shown in Figure 13. An example of a processed PIV velocity vector plot is shown in Figure 14. Note that due to the absence of seeding in the (red) region above the jet, these results should be discarded. From velocity vector plots like this, the mean jet trajectory height (middle of the jet region) and the height of the jet 'edge' (white area with zero velocity) were evaluated for conditions without a model. This information was used to estimate the effective shielding height of the air curtain, depending on tunnel velocity and jet velocity, in order to decide on interesting test conditions for a given half model behind the blowing slot.

#### E. Acoustic measurements

The acoustic measurements were done using a microphone array above the test section, which consisted of 80 1/2-inch microphones mounted in an open grid, and a total of 11 farfield microphones. In this way source locations and directivity could be measured. All microphones were equipped with wind screens. The array dimensions were chosen to be rather large (0.8 x 0.8 m<sup>2</sup>), in order to obtain high resolution at low frequencies. The array was placed outside the tunnel flow at a distance of about 0.8 m above the ground plate. The purpose of the additional far field microphones was to cover a larger range of directivity angles. Four microphones were mounted in a horizontal row on the ceiling above the tunnel flow, downstream of the microphone array (Figure 11). A vertical pole with seven microphones was placed downstream of the test section, either in the tunnel symmetry plane (for measurements without tunnel flow) or besides the test section at the same streamwise position (for measurements with and without tunnel flow).

The acoustic time data from the microphones was measured using a sample frequency of 51.2 kHz and a measurement time of 20 s. Before and after the measurements, the sensitivity at 1 kHz was checked for all array microphones using a calibrated pistonphone. Frequency-dependent sensitivities of individual microphones were taken from calibration sheets. No corrections were applied for microphone directivity since these effects are small for the present set-up. Phase matching of the microphones and correct location of noise sources was verified prior to the measurements by using a calibration sound source at different positions.

Conventional beamforming was used to obtain acoustic source maps in 1/3-octave bands. To improve the resolution and further suppress background noise from the tunnel, the main diagonal in the cross power matrix (autopowers) was discarded. The effect of sound refraction by the tunnel shear layer was corrected using a simplified Amiet method. The array scan plane, with a mesh width of 2.5 cm in both directions, was placed in the plane of the endplate. Example source maps are shown in Figure 15. Using the source maps, the noise from the model and air curtain could be separated from the extraneous noise of the wind tunnel. In order to quantify the model and blowing noise, an integration contour was defined around the complete model and blowing slot. The noise sources within the integration contour were quantified using a power integration method [11]. The source maps and integrated spectra will be presented in 1/3 octave bands at model scale frequencies, without A-weighting. The absolute levels are normalized to a reference distance of 0.282 m [ $(4\pi)^{-1/2}$ ], so that for a monopole source the peak level in the source map corresponds to the Sound Power Level (PWL).

Since all PIV measurements were done synchronously with the acoustic measurements, the possible influence of the PIV seeding on the acoustic results was verified by repeat measurements without seeding. In general the effect was found to be practically negligible, except at the highest frequencies for the lowest blowing speeds, where small differences (less than about 1 dB) were observed, which could be due to the (small) mass flow needed to inject the seeding in the pressure chamber.



## F. Test program

Several measurements were done for the four different slots (i.e. the 4-, 8-, and 11-mm normal blowing slots and the 8-mm oblique blowing slot). For each slot, first the 'blowing only' noise (without cross flow) was determined, as a reference and for comparison with literature. Next, the jets were measured in the presence of wind tunnel flow, to (1) determine the optimum blowing speed and model position for the subsequent measurements with model (on the basis of the shielding height observed in the PIV plots), and (2) to determine the effect of wind tunnel speed on the jet noise. After this, the performance of the air curtain was assessed by testing the models in the wind tunnel flow, with and without air curtain. In general two different model positions were tested: 12.5 and 17.5 cm behind the blowing slot for the 25-mm model, and 15 and 20 cm behind the blowing slot for the 50-mm model. Furthermore, for two slots the effect of flow deflectors on the curtain performance was investigated.

## IV. Results and discussion

In this section the aerodynamic and acoustic test results are presented and discussed. Section IVA describes the results for the isolated jets (without tunnel flow and without model). Section IVB deals with the results for the jets in cross-flow (without model). Finally, in Section IVC the performance of the air curtain is assessed in the presence of the half-models.

### A. Planar jets without cross-flow

For the measurements without tunnel flow, the array was directly exposed to the flow from the blowing slot. Despite the distorted signals on part of the array microphones, the microphone signals could still be used to produce acoustic source maps (not shown here), which gave qualitative information about the source characteristics. Thus, it could be concluded that in general the farfield noise was dominated by 2D slot noise.

For the *quantitative* analysis of single-microphone spectra, only the horizontal and vertical farfield microphones were used (Figure 11). In order to study the dependence of the jet noise on slot width and blowing speed, the most upstream horizontal microphone was used, which was mounted above the test section at  $\theta = 39^\circ$ , just downstream of the array. This microphone was not influenced by the jet flow or by possible reflections from the (lined) endplate, and had a fixed position during the complete test campaign (including the measurements with tunnel flow to be discussed in the next section). The other farfield microphones showed similar results; the directivity of the jet noise will be discussed below.

The measured spectra for the three different slot widths and different blowing speeds are shown in Figure 16 (left column). Whereas the spectra for the 8- and 11-mm slots exhibit one broad hump, the spectra for the 4-mm slot seem to be composed of a low- and high-frequency hump. The right column of Figure 16 shows the same spectra, but now normalized according to Eq. (2.12), with  $\xi = 8$  and  $\gamma = 0.75$ . The generic spectra obtained by Munro&Ahuja [8] for  $\theta = 90^\circ$  (see Figure 8) and  $\theta = 20^\circ$  are indicated by the solid black and red lines. It turns out that the high-frequency part of the  $h=4$  mm spectra collapses within a few dB, indicating that this part of the spectra scales with the 8<sup>th</sup> power of the jet speed. Moreover, a good agreement is found with the 90° spectrum from Ref. [8] (within a few dB). However, for the *low-frequency* part of the  $h=4$  mm spectra, and the complete 8- and 11-mm spectra, no good data collapse is observed, suggesting that the scaling from Ref. [8] is not appropriate.

If, instead of the 8<sup>th</sup> power, the 5<sup>th</sup> power (i.e.  $\xi = 5$ ) of the jet speed is used for the normalization, and  $\gamma = 1$ , *all* spectra collapse within about 5 dB (Figure 17), except obviously the high-frequency part of the high-speed 4-mm spectra. This suggests that there are two competing mechanisms which are responsible for the noise from the blowing slot: a high-frequency mixing noise component, which scales with the 8<sup>th</sup> power of the jet speed, and a low-frequency blowing slot edge noise mechanism, which scales with the 5<sup>th</sup> power of the jet speed [15]. Since the jet speeds in Ref. [8] were higher than 150 m/s, they only measured the mixing noise component, while in the present study edge noise appears to be dominant for blowing speeds below 140 m/s ( $M_j = 0.4$ ). Previous studies have also found powers  $\xi$  lower than 8 for jets at relatively low speeds, which were sometimes attributed to edge or 'lip' noise [12-14]. For a high-aspect ratio planar jet, this edge noise component can be expected to be more important than for a round jet, due to the larger edge/area ratio. It is important to note in Figure 16 that, due to this deviation from the generic spectra from Ref. [8], the blowing slots are generally noisier than anticipated during the design study described in Section II.

Also note that in Figure 17 the best data collapse was obtained when, instead of the value  $\gamma = 0.75$  used in Ref. [8],  $\gamma = 1$  was used for the normalization according to Eq. (2.12). In the present tests the slot length  $w$  was the same in all cases, so that in the level and frequency normalization only the power for the slot width  $h$  was relevant.



Thus, for the edge noise mechanism the acoustic intensity appears to be proportional to the square of the slot width, and the frequency appears to be inversely proportional to the slot width.

In order to study the directivity of the jet noise, all horizontal and vertical farfield microphones (Figure 11) were used. Figure 18 shows the measured and normalized spectra on all farfield microphones for the 4-mm slot at the highest and lowest jet speed. Note that the vertical microphones correspond to channels 81 (bottom) to 87 (top), and the horizontal microphones to channel numbers 88 (upstream) to 91 (downstream). For the highest jet speed, where the mixing noise mechanism is relatively important, the normalization (including directivity correction) results in a good collapse (within about 5 dB, see top-right figure in Figure 18) of the spectra for the different radiation directions. Thus, the directivity scaling of levels and frequency according to Ref. [8] appears to be valid for this case, i.e. the smaller  $\theta$ , the lower the peak frequencies and the higher the peak level. However, for the *low* jet speed, where the edge noise mechanism is dominant, the directivity scaling does not significantly improve the data collapse. Also for the other slot widths, even at the highest jet speed, only a marginal improvement was observed in the data collapse after applying the directivity normalization. This suggests that the edge noise mechanism has a different directivity pattern than the mixing noise mechanism.

### B. Planar jets in cross-flow

The effect of tunnel flow on jet noise is illustrated in Figure 19, which shows the measured spectra at the same microphone as in the previous section, i.e. the most upstream horizontal far field microphone at  $\theta = 39^\circ$ . The trends were generally the same on the other far field microphones. In the left column it can be seen that for practically all jet speeds and slot widths the jet noise increases when 50 m/s tunnel flow is introduced. The noise increase with respect to zero tunnel flow ranges between about 2-3 dB for the 11-mm slot to more than 5 dB for some jet speeds of the 4-mm slot. The right column shows that the jet noise increases with tunnel flow speed: for the 8- and 11-mm slots an increase in tunnel speed from 35 to 50 m/s, or from 50 to 70 m/s, gives an increase of about 3-4 dB. For the 4-mm slot the noise increase depends strongly on frequency: a large increase is observed at low and high frequencies and almost no increase at medium frequencies.

The noise increase due to cross-flow may be partly explained by the increased noise source levels at the slot corners for the lower blowing speeds (Figure 20). These edge sources were not visible in the source maps without cross-flow. This suggests that this noise is due to some interaction between the tunnel and slot flow, e.g. by the curvature of the tunnel flow around the planar jet.

In the following the *aerodynamic* results for the planar jets in cross-flow are discussed. The jet centerline trajectory was estimated on the basis of the PIV images (see examples in Figure 13 and Figure 14). According to Eq. (2.2), the centerline height  $x$  at a given downstream position  $y$  should be proportional to  $R\sqrt{hy}$ . Figure 21 shows that Eq. (2.2) applies well for all three normal blowing slots, provided that the proportionality constant  $c_j$  is taken equal to 1.5 instead of 1.2. This higher value may be due to 3D effects: due to the open jet configuration the tunnel flow may be deflected sideways, enabling a higher jet trajectory than in a 2D set-up. Note that the higher value for  $c_j$  implies that the required blowing speeds for a given shielding height are lower than anticipated during the design study described in Section II. Also note that the 4-mm slot was tested up to very high values of  $R$ , for which the jet trajectory height covers a substantial part of the tunnel nozzle height. Under these conditions the jet trajectory height no longer scales linearly with  $R$ .

The effect of a 25-mm quarter-circle flow deflector (Figure 7) is shown in Figure 22. It can be seen that the deflector leads to higher jet trajectories, especially at low  $R$ . The aerodynamic effect of a flow deflector was estimated in Section IIA, Eq. (2.6), and it can be seen that this simple model reasonably well fits the experimental data when taking  $c_v = 0.3$  (and  $c_j = 1.5$ ). In particular the model explains the decrease in deflector benefit for larger values of  $R$ .

The effect of oblique blowing (Figure 6) is shown in Figure 23. It can be seen that oblique blowing results in much higher jet trajectories than for the corresponding normal blowing slot. The aerodynamic effect of oblique blowing was estimated in Section IIA, Eq. (2.8), and it can be seen that this simple model shows the same trend as the experimental data (again  $c_j = 1.5$  and  $c_v = 0.3$ ). In particular the model shows the progressive increase in jet height with  $R$ .

The effect of inflow turbulence was assessed by mounting a turbulence grid in the wind tunnel nozzle, but no significant effect was found on the trajectory (or noise) of the jets.

### C. Noise reduction potential

In this section the ability of the air curtain to reduce the noise from the different bluff bodies will be assessed. First, the procedure that was used to determine the optimum model position and blowing speeds is described. Next, the performance of the normal blowing slots is addressed. Finally, the results for the oblique blowing slot and flow deflectors are discussed.

#### 1. Determination of model positions and blowing speeds

The model positions and blowing speeds were determined on the basis of the PIV results discussed in the previous section (i.e. without model). First, for both model heights (25 mm and 50 mm) a value of the velocity ratio was selected for which the jet 'edge' (see Section IIID) was just higher than the model. Using tunnel speeds of 50 and 70 m/s, this leads to two blowing speeds. By adding one intermediate blowing speed, a total number of six test conditions was obtained, with five different values of  $R$ . An example is given in the table below.

**Table 1: Example of test conditions for a given slot width (4 mm) and model height (50 mm).**

<b>R</b>	2	2.4	<b>2.8</b>	<b>2.8</b>	3.36	3.92
<b>V<sub>j</sub></b>	140	168	196	140	168	196
<b>V</b>	70	70	70	50	50	50

The selected value of  $R = 2.8$  is tested at both wind tunnel speeds. In addition, two lower  $R$ -values are tested at 70 m/s and two higher values are tested at 50 m/s. Note that the selected  $R$ -value is different for different model heights and/or different slot widths. Since for near-optimum conditions the height of the jet edge did not vary a lot in streamwise direction, two fixed model (leading edge) positions were selected: 12.5 and 17.5 cm behind the blowing slot for the 25-mm model, and 15 and 20 cm behind the blowing slot for the 50-mm model.

#### 2. Assessment of air curtains with normal blowing

As an example, Figure 24 shows typical acoustic source maps and PIV plots for the 50-mm model behind the 11-mm slot at different blowing speeds. Since the seeding was injected through the blowing slot, there is no PIV plot for the reference case without blowing. In the acoustic source maps, tunnel flow is from left to right, the black contours indicate nozzle, endplate, blowing slot and model, and the range of the color scale is 12 dB (same color scale for all maps). The air curtain is seen to reduce the model noise, and the jet noise increases with blowing speed. Interestingly, the best acoustic result is obtained for the lowest blowing speed, where the curtain seems to hit the model. This is quite surprising, especially since inspection of individual PIV plots showed significant flow unsteadiness. Apparently, the average flow speed at the model is low enough to reduce the model noise.

A quantitative assessment of the air curtains was made in terms of integrated array spectra, using the integration contour shown in Figure 15 (including slot, model, and possible edge sources). These spectra exclude possible tunnel noise, and have a higher signal-to-noise ratio than single-microphone spectra. Integrated spectra for the 11-mm slot are shown in Figure 25. The acoustic performance of the air curtains can be assessed by comparing the colored lines (with air curtain) to the solid black line (reference case). This figure confirms that the best results are obtained at the lowest blowing speeds, i.e. the lowest values of  $R$ . Apparently the selected  $R$ -value on the basis of the no-model measurements was too high. Since the lower  $R$ -values are only tested at 70 m/s tunnel speed (Table 1), the best results are obtained for 70 m/s wind speed. If we compare the results for the *same*  $R$ -value (the blue line at 50 m/s and the red line at 70 m/s), the reductions are similar.

If we compare the two lower plots in Figure 25 (both at 70 m/s), we see that the largest noise reduction is obtained for the 25-mm model. This is because higher blowing speeds are required to shield the 50-mm model, which leads to substantially higher blowing noise levels, while the baseline 50-mm model is not much noisier than the 25-mm model. Since in the design study (Section II) the spectrum of a full-model H-strut (5 cm wide) was used as a reference (Figure 10), it is interesting to compare the noise from the present half-models to that strut. For this purpose, the grey line in the lower left plot of Figure 25 indicates the spectrum of the H-strut. This H-strut spectrum was normalized to the same distance and model length as in the present tests, and 3 dB was subtracted to account for the present half-model set-up (actually 3 dB should be added to the blowing noise to account for the second slot that would be needed to shield the full-model H-strut, but instead here 3 dB was subtracted from the H-strut spectrum). It can be seen that the present half-model is significantly quieter than the full-model H-strut. Not only the



low-frequency alternating vortex shedding peak (not visible in Figure 25) has disappeared completely, but also the broadband noise levels at higher frequencies are much lower. So if we assume that the present jet speeds would be enough to shield half the H-strut, drastic noise reductions (up to about 10 dB) would be possible with a two-slot blowing device upstream of the full-model H-strut. Thus, while for the relatively quiet half-models in the present study a broadband noise reduction of 3-5 dB is obtained, for full models larger reductions may be expected. The effect of model geometry on noise reduction will be further investigated below.

The effect of model position is illustrated in Figure 26. Comparison of the two plots shows that the downstream model position gives slightly better results. By comparing the right plot in Figure 26 to the lower left plot in Figure 25, we can see that the results for the 11-mm slot are better than for the 8-mm slot. This is because the required blowing speeds are higher for the 8-mm slot, as anticipated during the design study. In summary, for the normal blowing slots, the largest noise reductions are obtained for the lowest model height (25 mm), the largest slot width (11 mm), the lowest blowing speed (59 m/s at 70 m/s tunnel speed), and the downstream model position (175 mm behind the slot).

As mentioned above, the half-models in the present study were relatively quiet. Thus, in order to obtain a noisier, more realistic baseline, the 25-mm and 50-mm models were combined by placing the smaller model upstream of the larger model (with a 25-mm gap). The integrated spectra for this combined model, with and without the 11-mm air curtain, are shown in Figure 27. By comparing this plot to the lower right plot in Figure 25, we see that the noisier baseline model indeed leads to larger noise reductions: whereas for the single 50-mm model reductions are obtained only at the higher frequencies, for the combined model a broadband noise reduction of about 3 dB is achieved.

### 3. Effects of oblique blowing and flow deflectors

For the 8-mm oblique blowing slot the trends were the same as for the normal slots: the best results were obtained at a tunnel speed of 70 m/s (i.e. lowest  $R$ -values), for the downstream model position. However, due to the fact that the required jet velocity for a given shielding height is lower than for the 8-mm normal slot (Section IVB), larger noise reductions can be anticipated. The integrated spectra for the 25- and 50-mm models at the downstream position for 70 m/s wind speed are shown in Figure 28. For the 25-mm model broadband noise reductions up to more than 5 dB are obtained for the important frequencies at the lowest blowing speed, although below 1 kHz a small noise increase occurs. The reductions are indeed higher than for the 8-mm normal slot (Figure 26). For the full-model H-strut reductions up to more than 10 dB may be anticipated. For the 50-mm model, smaller noise reductions are observed than for the 25-mm model. Figure 15 shows source maps for the 50-mm model with the oblique slot, at a tunnel speed of 70 m/s and a blowing speed of 83 m/s.

For the 11-mm normal blowing slot, the effect of flow deflectors (Figure 7) directly behind the slot was tested. The idea was that using a flow deflector, lower blowing speeds are required for a given shielding height (see Section IVB), thus increasing the noise reduction. The deflectors were only tested with the 50-mm model. The integrated spectrum for the 25-mm quarter-circle deflector at 70 m/s tunnel speed is given in Figure 29 (left plot). It can be seen that even without blowing the deflector already yields a noise reduction at higher frequencies. When the blowing is switched on, the noise reduces further to obtain a broadband reduction of up to about 10 dB. In order to check the sensitivity to the shape of the deflector, a 25-mm simple (non-streamlined) L-shaped deflector was tested as well (right plot in Figure 29). The results are very similar to the quarter-circle deflector, indicating that the *shape* is not very critical. However, when a 10-mm L-shaped deflector was used (not shown), the results were clearly worse, which shows that the *height* of the deflector is important.

## V. Conclusion

Acoustic and aerodynamic measurements were performed in NLR's Small Anechoic Wind Tunnel on the air curtain concept, which is intended for landing gear noise reduction. The idea of this concept is to apply an upstream blowing slot to deflect the flow around a landing gear (component), thus reducing the local flow speeds and therefore the aerodynamically generated noise. Prior to the wind tunnel tests, a design study was carried out to assess the possible benefit of an air curtain. On the basis of the available literature for planar jets in cross-flow, the required jet exhaust velocity and mass flow for obtaining a certain shielding height were estimated as a function of slot width. Next, the noise production of the air curtain was estimated on the basis of previous aeroacoustic studies into planar jets (without cross-flow), and compared to the noise production of a generic strut measured in an earlier test campaign. This study showed that it is in principle possible to obtain a substantial noise reduction using an air curtain. The pre-test estimations showed that, for a given shielding height, increasing the slot width results in lower noise levels (due to the lower blowing speeds) but higher required mass flows. Based on these findings a test set-up and test program were defined for the wind tunnel measurements.





In the subsequent proof-of-concepts tests, two-dimensional half-models were mounted on an acoustically lined endplate which was attached to the lower edge of the wind tunnel nozzle. Blowing was applied through a slot in the endplate, upstream of the model. The pressurized air supply system was acoustically treated to suppress possible extraneous noise. Microphone array and PIV measurements were performed to characterize the acoustics and aerodynamics of the air curtain. Tests were done for different wind tunnel speeds, blowing speeds, slot geometries and model geometries.

The test results for the isolated planar jets (without tunnel flow) showed that for the highest blowing speeds the noise spectra agreed well (within a few dB) with results reported in literature. For these cases the noise levels scaled with the 8<sup>th</sup> power of the jet speed. However, for the lower jet speeds, which were most relevant for the subsequent air curtain tests, the blowing slot noise was found to scale with the 5<sup>th</sup> power of the jet speed, suggesting that, rather than jet mixing noise, edge noise was the dominant mechanism. As a result the isolated blowing slot was significantly noisier than expected on the basis of the design study. The supposed dominance of the edge noise mechanism may be explained by the relatively low jet Mach numbers and the relatively large edge/area ratio of the rectangular blowing slot (as compared to a round nozzle). For the highest blowing speeds (mixing noise) the directivity of the slot noise agreed with literature, but for the lower jet speeds (edge noise) a different directivity pattern was found. The noise levels for the isolated planar jets were found to scale with the square of the slot width.

The results for the jets in cross-flow showed that addition of 50- or 70-m/s wind tunnel flow increased the jet noise levels by about 3 or 6 dB, respectively, for the relevant slot widths. The acoustic source maps indicated that this noise increase may be partly explained by increased sound levels at the corners of the slot, especially for the lower blowing speeds. The aerodynamic results showed that the dependence of the air curtain trajectory on wind speed, blowing speed, and slot width was as expected on the basis of the literature. However, the shielding height was consistently 25% higher than anticipated, which means that for a given shielding height the required jet speed was lower. The increased shielding height may be due to 3D effects: due to the open jet configuration the tunnel flow may be deflected sideways, enabling a higher jet trajectory than in a 2D set-up.

The test results for the normal blowing slots in combination with a half-model showed that the largest noise reductions were obtained for the lowest model height (25 mm), the largest slot width (11 mm), the lowest blowing speed (59 m/s at 70 m/s tunnel speed), and the downstream model position (175 mm behind the slot). For this case broadband noise reductions of 3-5 dB were obtained. It was quite surprising that the lowest blowing speed gave the best results, since according to the PIV results the (unsteady) curtain seemed to hit the model for these conditions. Apparently, the average flow speed at the model was still low enough to reduce the model noise. Since the baseline rectangular half-models in the present tests were much quieter than a full-model generic strut measured in an earlier test campaign, reductions of 5-10 dB may be expected when a normally blowing air curtain is applied to a full-model. This hypothesis was supported by measurements on a noisier baseline model, which exhibited larger noise reductions.

When oblique blowing (30° upstream) was applied, lower blowing velocities were needed to achieve a certain shielding height. As a result, the noise reduction could be increased by several dB's with respect to normal blowing, at the expense of a slight noise increase at low frequencies (below 1 kHz). Similarly, the use of a flow deflector directly in front of the blowing slot increased the shielding height and therefore the noise reduction. For a 25-mm quarter-circle deflector in combination with a 50-mm model, broadband noise reductions of 5-10 dB were obtained. A simple L-shaped deflector with the same height gave the same results. For the same 50-mm model, smaller noise reductions were achieved when the deflector height was reduced to 10 mm.

### Acknowledgments

This study was carried out in the framework of the European research project TIMPAN (Technologies to Improve Airframe Noise), which is part of the sixth framework programme. This project is funded by the European Commission and is coordinated by Airbus France. The contribution of the project partners to the definition of the experiments and the interpretation of the results is highly appreciated.

### References

- <sup>1</sup> Gutmark, E., Wagnanski, I., The planar turbulent jet, *Journal of Fluid Mechanics*, Vol. 73, 1976.
- <sup>2</sup> Guyonnaud, L., Solliec, C., Dufresne de Virel, M., Rey, C., Design of air curtains used for area confinement in tunnels, *Experiments in Fluids* 28, 2000.
- <sup>3</sup> Drotz, A., Greiveldinger, B., Sawley, M.L., Numerical flow simulation of an air curtain for road tunnel fire security, EPFL, 2004.



- <sup>4</sup> Ramaprian, B.P., Haniu, H., Turbulence measurements in plane jets and plumes in crossflow, IHR Report No. 266, Iowa Institute of Hydraulic research, 1983.
- <sup>5</sup> Vincenti, I., Guj, G., Camussi, R., Giulietti, E., PIV study for the analysis of planar jets in cross-flow at low Reynoldsnumbers, 11th National Convention AIVELA, Ancona, Italy, 2003.
- <sup>6</sup> Olsen, W.A., Guerrez, O., Dorsch, R.G., The effect of nozzle inlet shape, lip thickness, and exit shape and size on subsonic jet noise, AIAA paper 73-187, 1973.
- <sup>7</sup> Kouts, C., Yu, J.C., Far noise field of a two-dimensional subsonic jet, AIAA paper 74-44, 1974.
- <sup>8</sup> Munro, S.E., Ahuja, K.K., Aeroacoustics of a high aspect-ratio jet, AIAA paper 2003-3323, 2003.
- <sup>9</sup> Munro, S.E., Ahuja, K.K., Development of a prediction scheme for high aspect-ratio jet noise, AIAA paper 2003-3255, 2003.
- <sup>10</sup> Ahmed, K.A., Forliti, D.J., Moody, J.K., Yamanaka, R., Flowfield Characteristics of a confined transverse slot jet, AIAA journal, Vol. 46, No. 1, 2008.
- <sup>11</sup> Oerlemans, S., Broersma, L., Sijtsma, P., Quantification of airframe noise using microphone arrays in open and closed wind tunnels, International Journal of Aeroacoustics Vol. 6-4, 2007.
- <sup>12</sup> Ahuja, K.K., Bushell, K.W., An experimental study of subsonic jet noise and comparison with theory, Journal of Sound and Vibration, 30(3), 1973.
- <sup>13</sup> Gruschka, H.D., Schrecker, G.O., Aeroacoustic characteristics of jet flap type exhausts, AIAA paper 72-130, 1972.
- <sup>14</sup> Olsen, W., Karchmer, A., Lip noise generated by flow separation from nozzle surfaces, NASA TM X-71859, AIAA paper 76-3, 1976.
- <sup>15</sup> Blake, W.K., Mechanics of flow-induced sound and vibration, Academic Press, 1986.

Figures

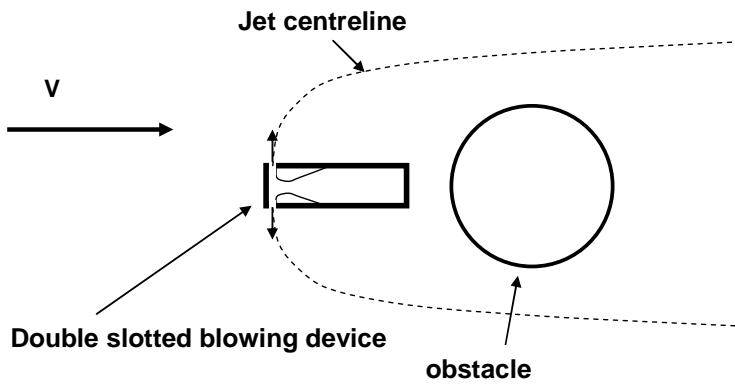


Figure 1: Sketch of a double-slotted air curtain device shielding a cylindrical obstacle.

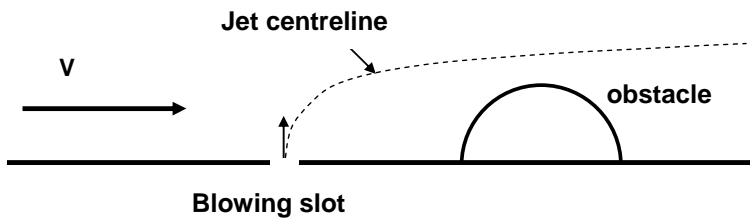


Figure 2: Half-model implementation of air curtain device used in the experiments.

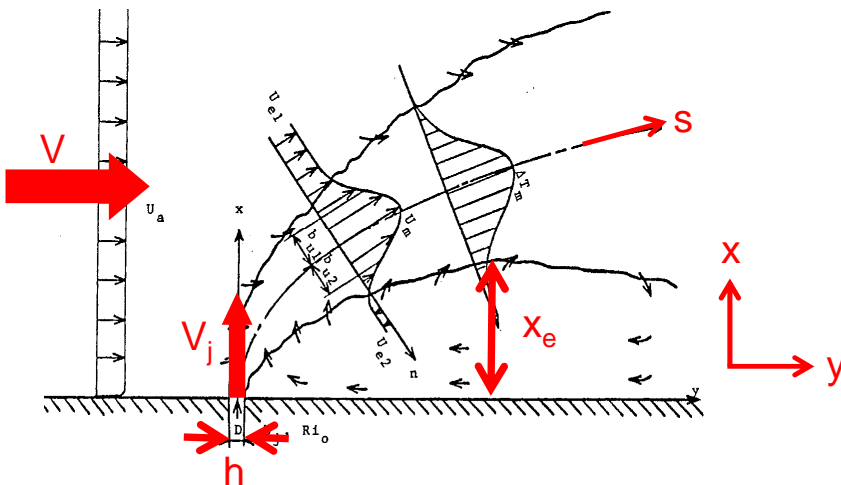


Figure 3: Schematic view of planar jet in cross-flow [4] and definition of coordinates for present study (red).

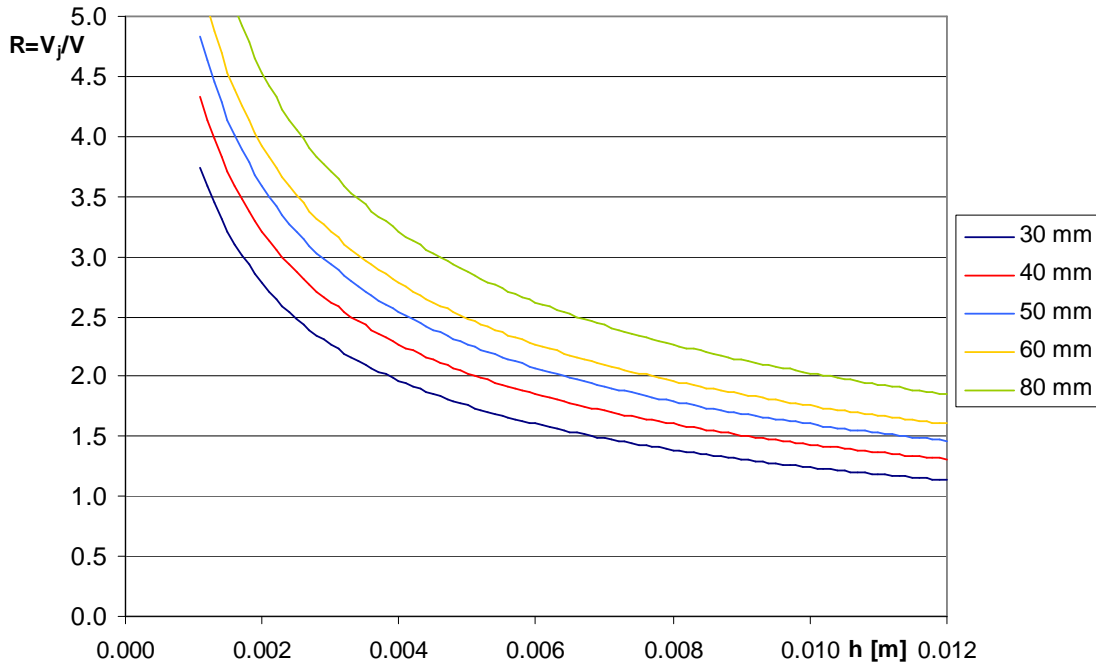


Figure 4: Estimated required jet velocity as function of the width  $h$  for a normally blowing air curtain device, for different effective shielding heights  $x_e$ .

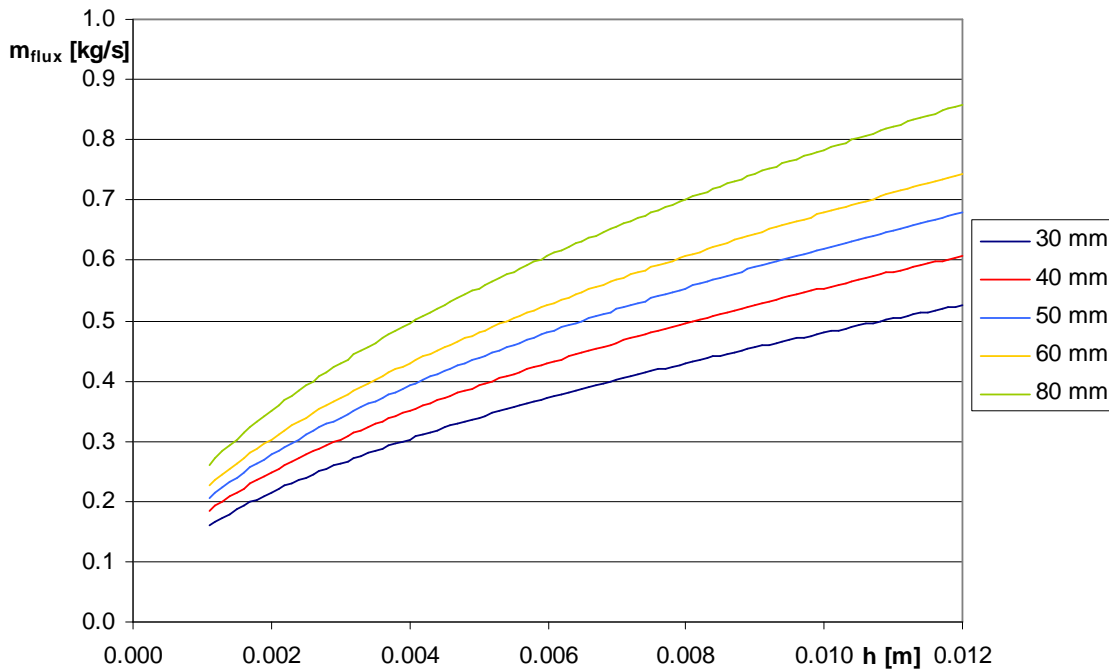


Figure 5: Estimated required mass flux as function of slot width  $h$  for a normally blowing air curtain device, for different effective shielding heights  $x_e$ .

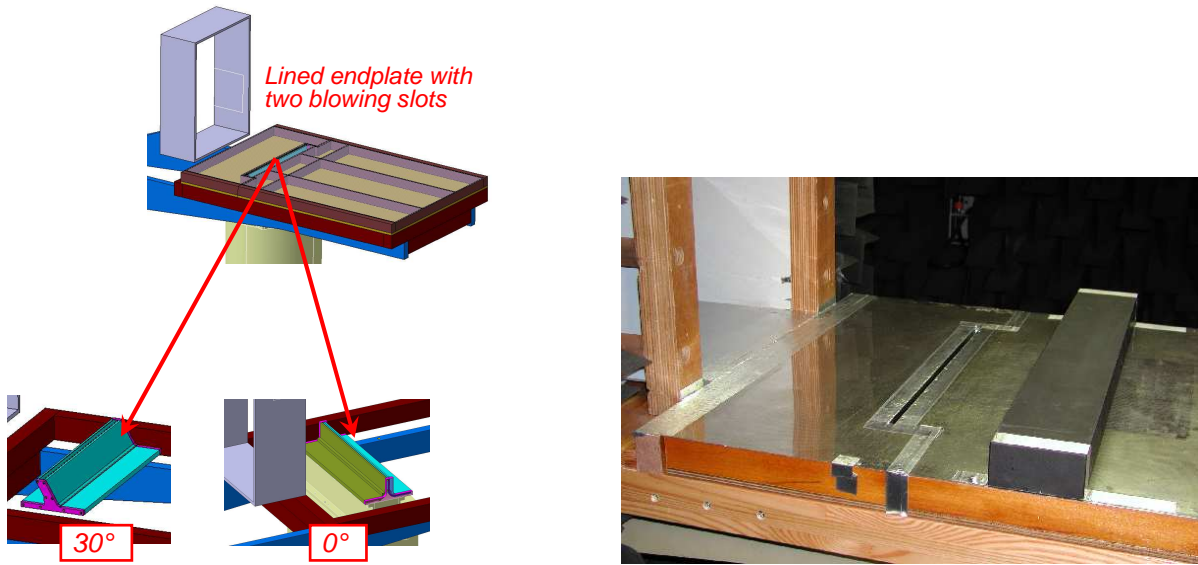


Figure 6: Picture of oblique and normal blowing slots (left), and close-up of model and blowing slot (right).

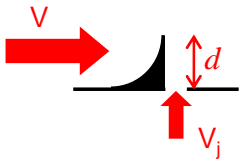


Figure 7: Quarter-circle flow deflector just upstream of the blowing slot.

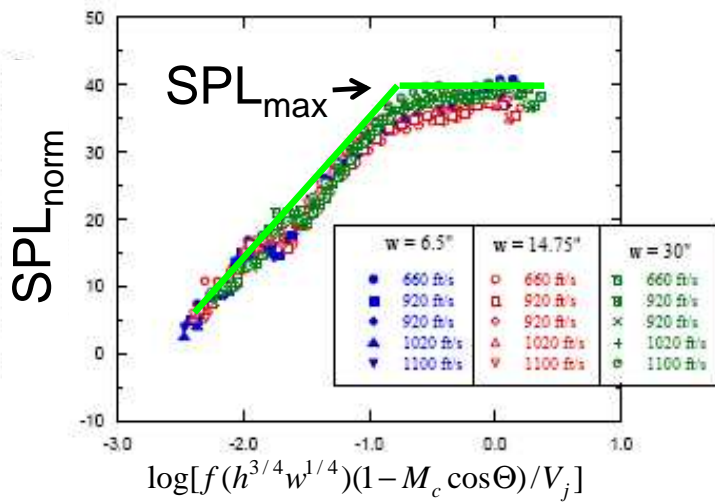


Figure 8: Normalized acoustic spectra for high aspect ratio nozzles [8].

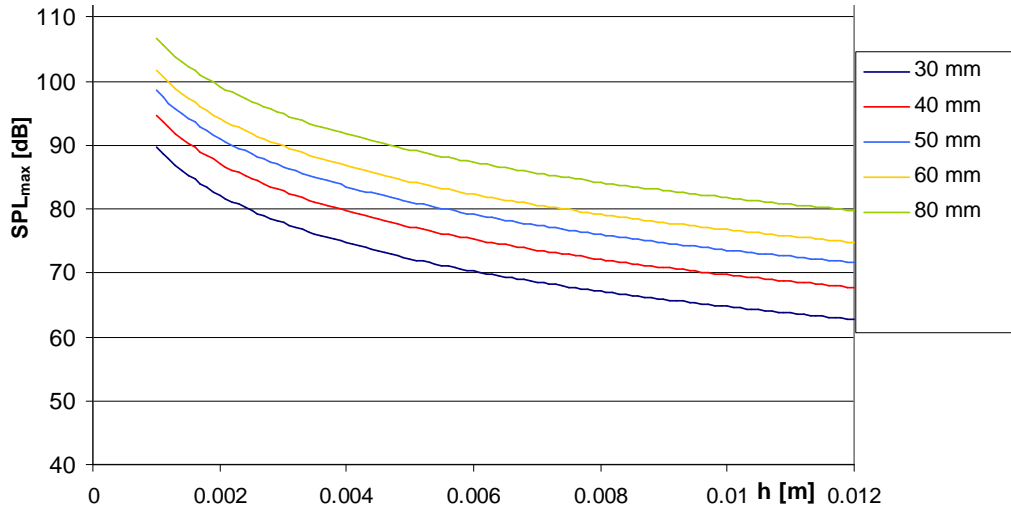


Figure 9: Estimated  $SPL_{max}$  as function of slot width  $h$  for a normally blowing air curtain device, for different effective shielding heights  $x_e$ .

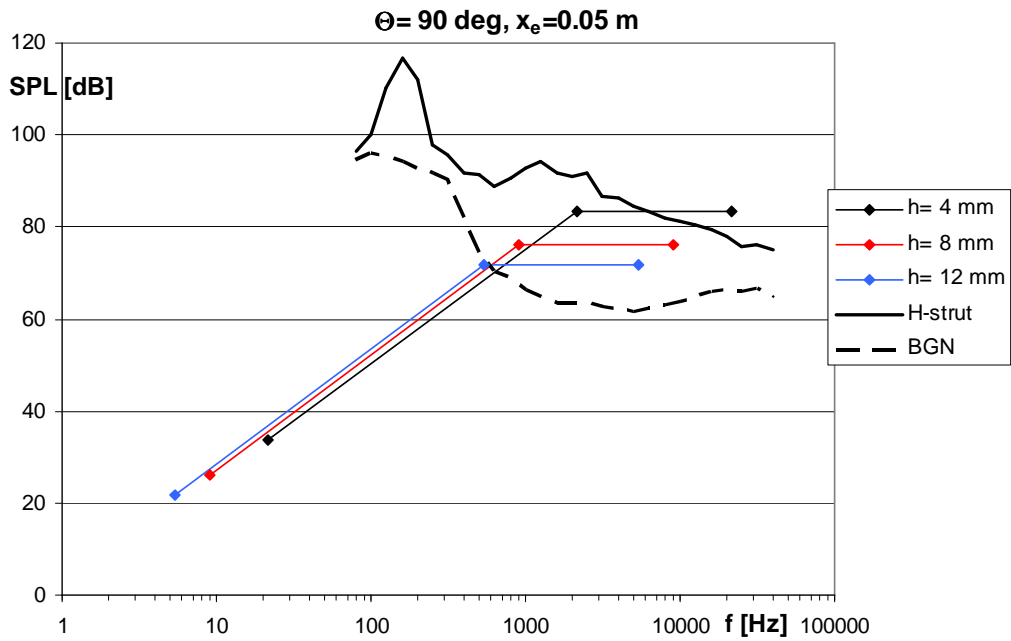


Figure 10: Comparison between measured spectrum of a 5-cm H-strut and estimated spectra for a normally blowing air curtain device with a shielding height of 5 cm, for different slot widths.

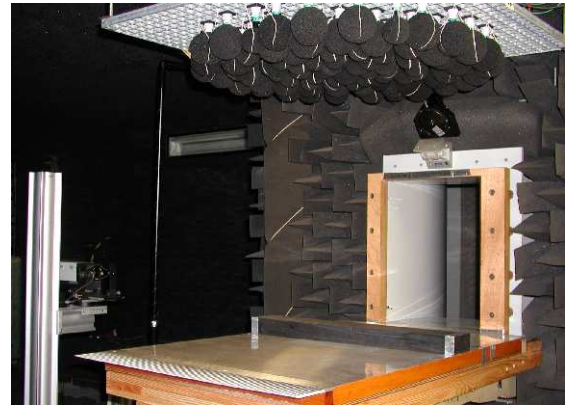
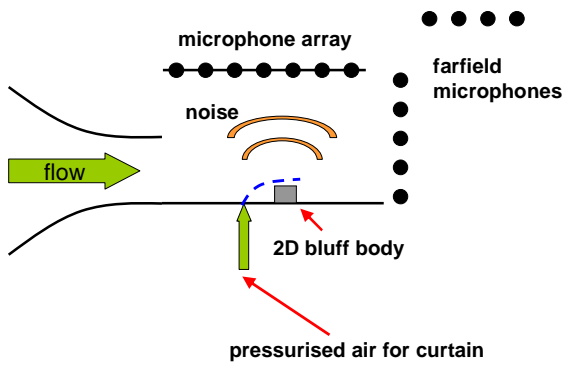


Figure 11: Schematic picture of test set-up and photograph with nozzle, endplate, model, array, and PIV camera.

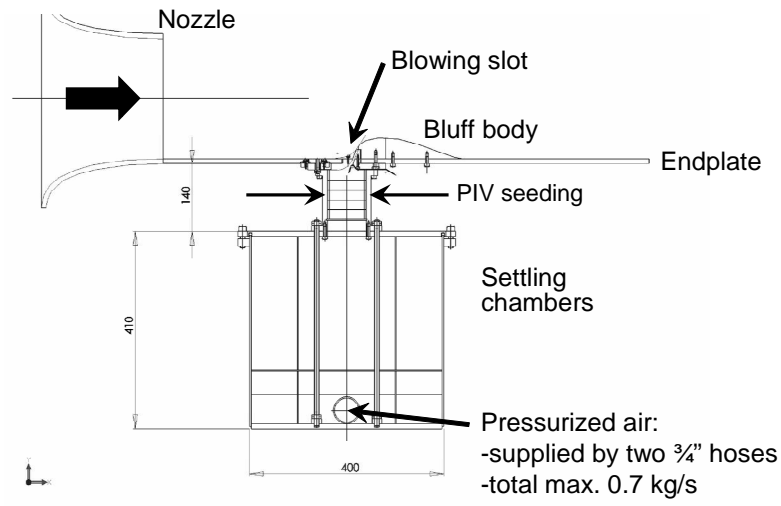


Figure 12: Blowing system.

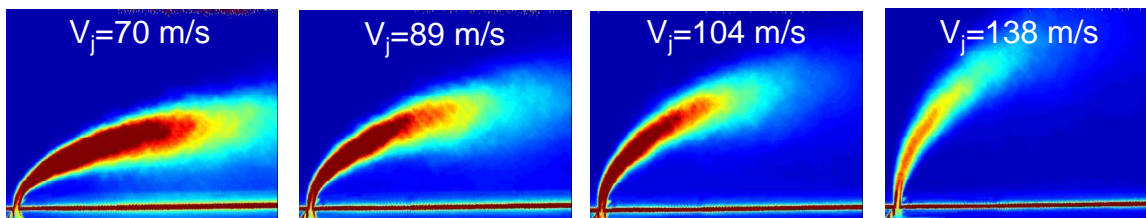


Figure 13: Example averaged PIV seeding intensity maps for a wind tunnel speed of 35 m/s and different blowing speeds.

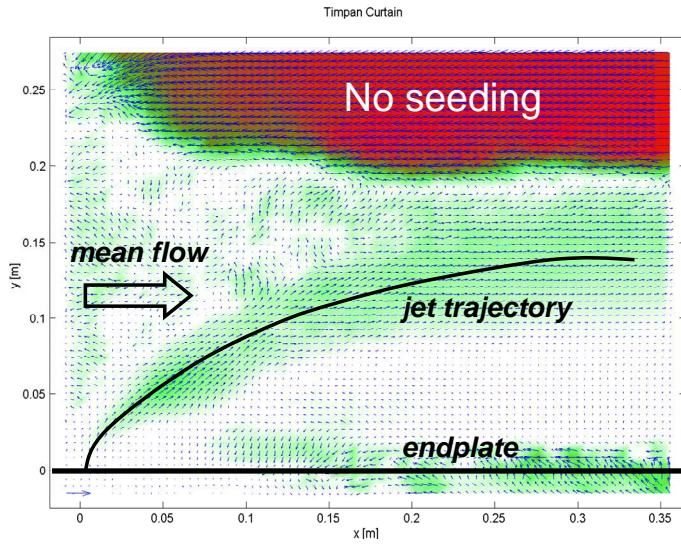


Figure 14: Example of mean velocity vectors for 8-mm normal blowing slot with a wind tunnel speed of 35 m/s and a blowing speed of 70 m/s.

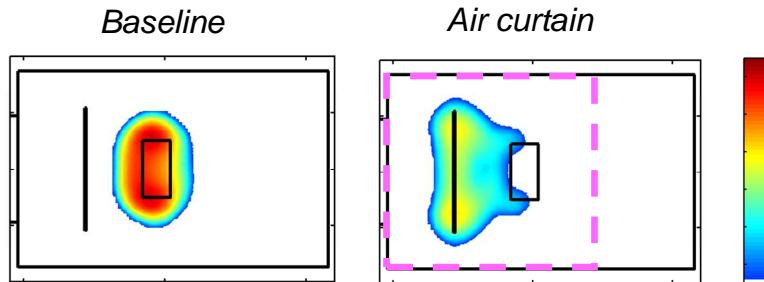
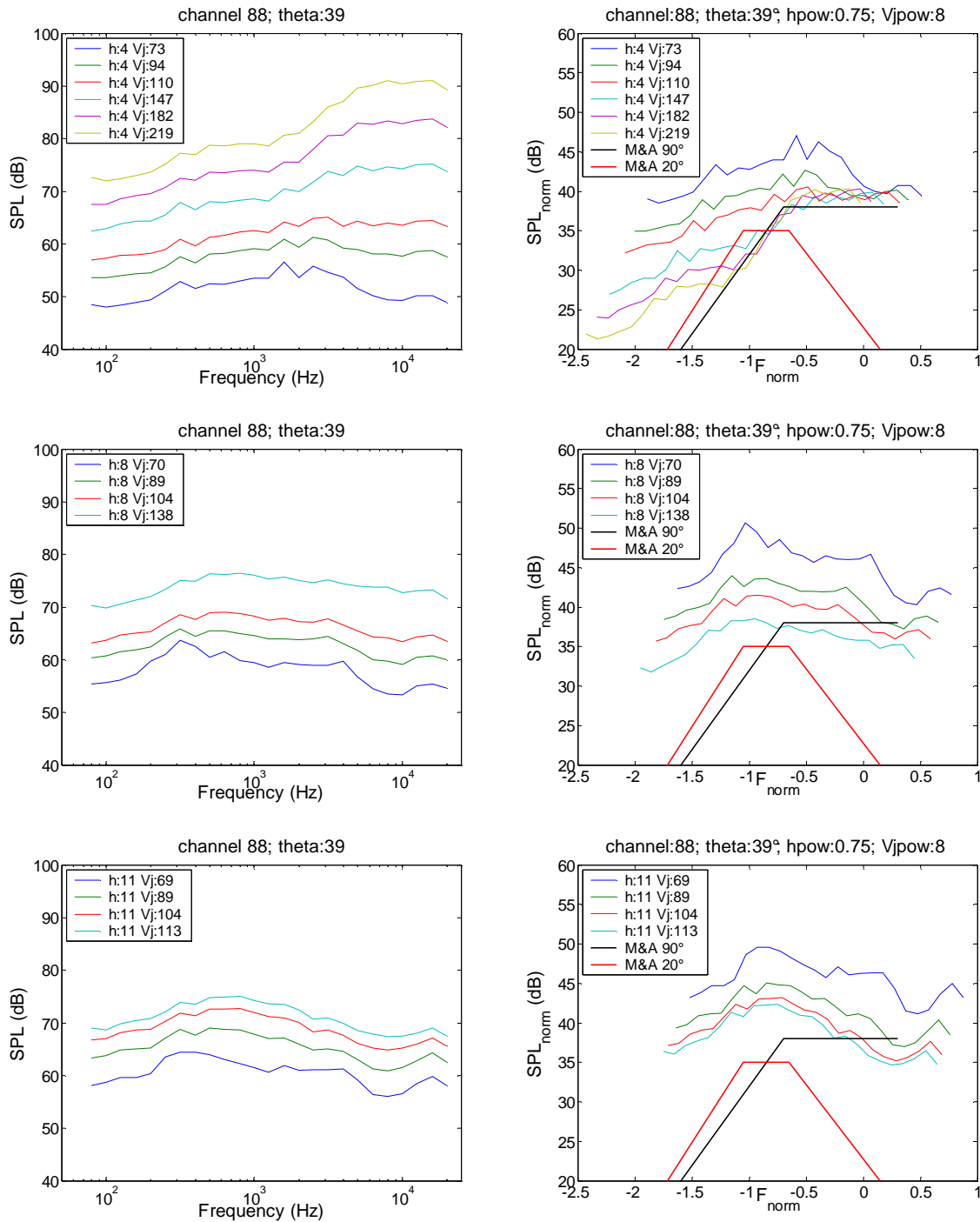


Figure 15: Example acoustic source maps (4 kHz) for rectangular half-model (5 cm high) at 70 m/s wind speed, without (left) and with (right) air curtain. Tunnel flow is from left to right and the black contours indicate nozzle, endplate, blowing slot and model. The pink dashed contour indicates the power integration region. The range of the color scale is 12 dB.





**Figure 16: Dimensional (left) and normalized (right) jet noise spectra (without cross-flow), for three slot widths (normal blowing) and varying jet velocity  $V_j$ . The normalization was done using Eq. (2.12) with  $\xi = 8$  and  $\gamma = 0.75$ , in accordance with Munro&Ahuja [8].**

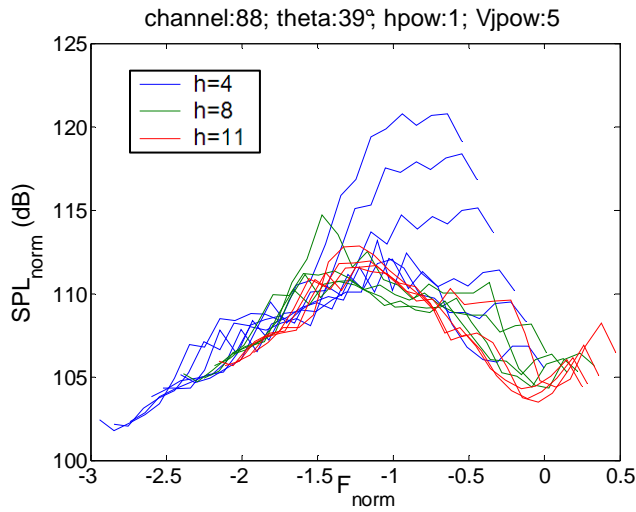


Figure 17: Normalized jet noise spectra (without cross-flow), for three slot widths (normal blowing) and different jet velocities  $V_j$ . The normalization was done using Eq. (2.12) with  $\xi = 5$  and  $\gamma = 1$ .

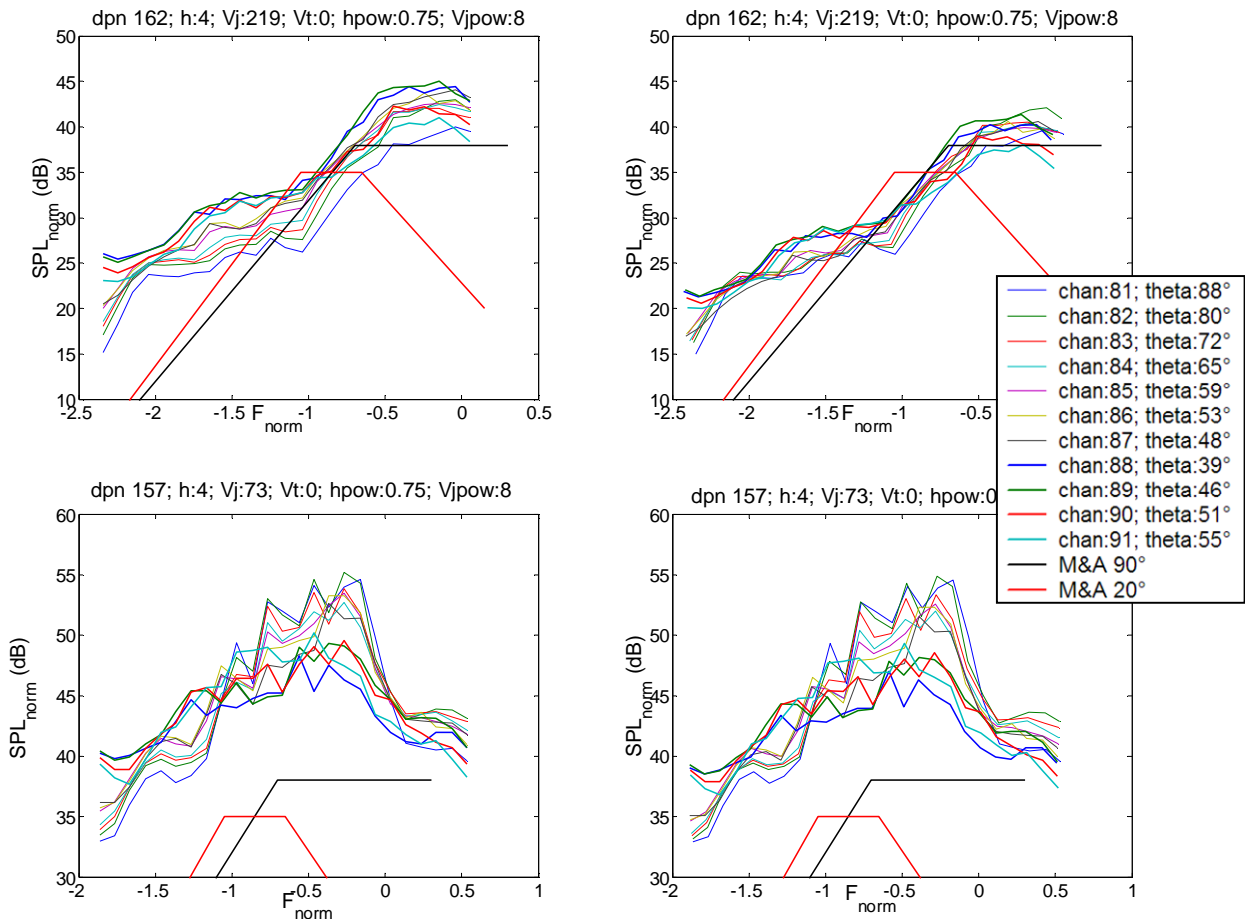
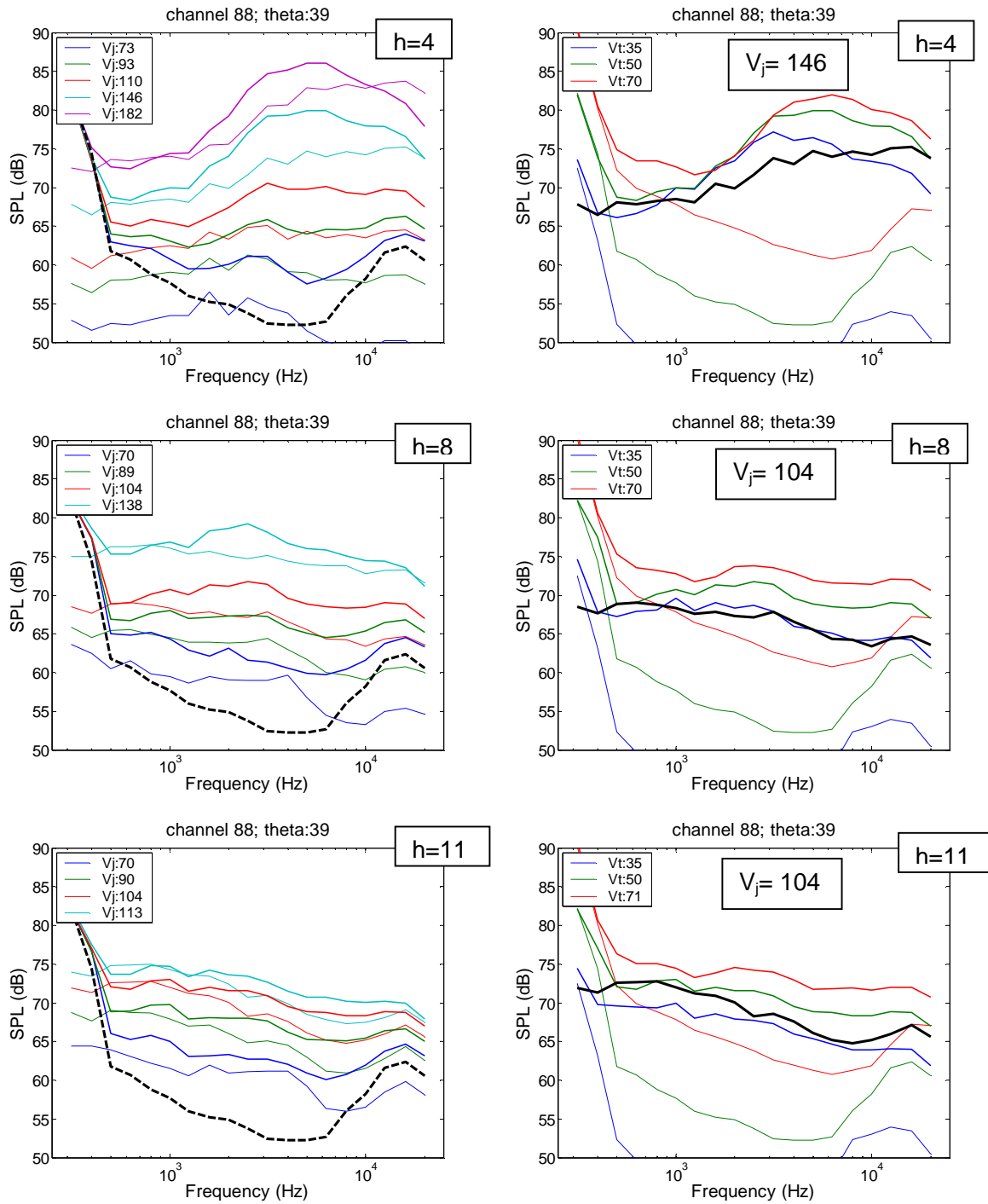


Figure 18: Normalized farfield jet noise spectra (without cross-flow) for the 4-mm slot at jet velocities of 219 m/s (upper row) and 73 m/s (lower row). The normalization was done using Eq. (2.12), without (left) and with (right) the  $\theta$ -factor.



**Figure 19: Effect of wind tunnel flow on jet noise.** In the left column the thin lines are without tunnel flow, the bold lines for  $V = 50$  m/s, and the dashed line indicates the tunnel background noise at 50 m/s. In the right column the thin lines indicate the tunnel background noise at three wind speeds, the bold lines show the jet noise for different tunnel flow speeds, and the black line indicates the 'blowing only' noise (without cross-flow).

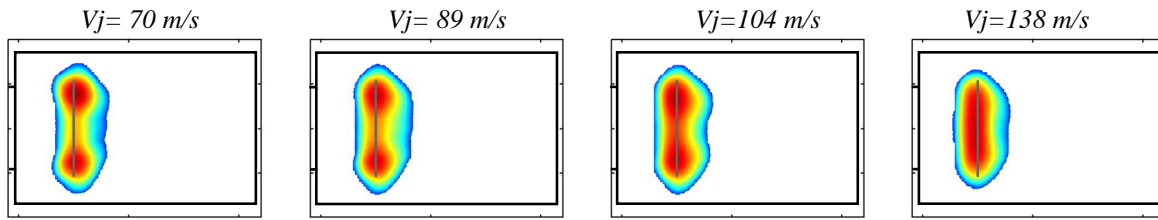


Figure 20: Source maps (4 kHz) for 8-mm jet with 70 m/s tunnel flow, at different jet speeds.

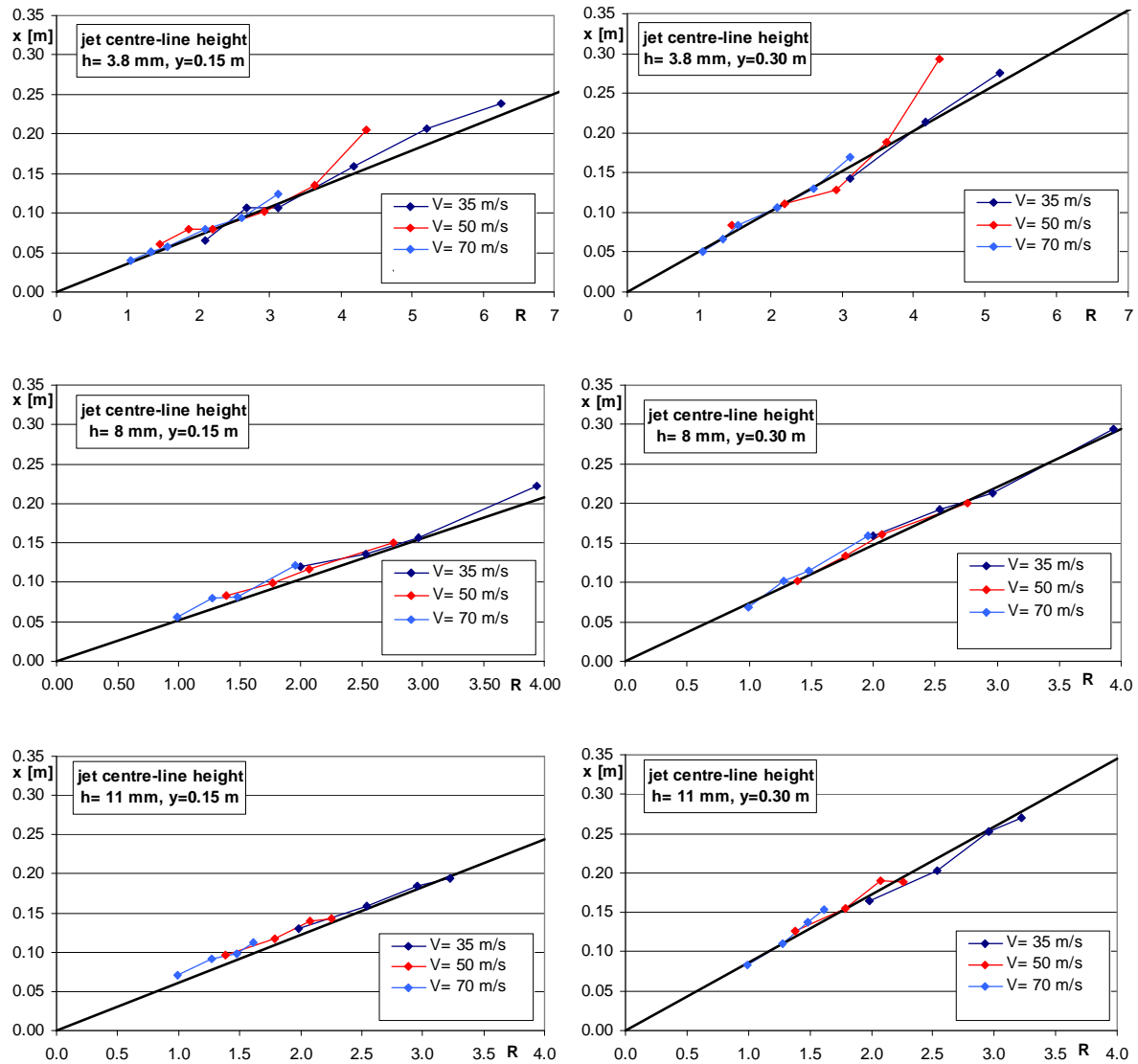


Figure 21: Jet centerline height as a function of velocity ratio  $R$ , at streamwise distances of  $y = 0.15$  (left) and  $y = 0.30$  (right). The black line shows the relationship according to Eq. (2.2), with  $c_j = 1.5$ .

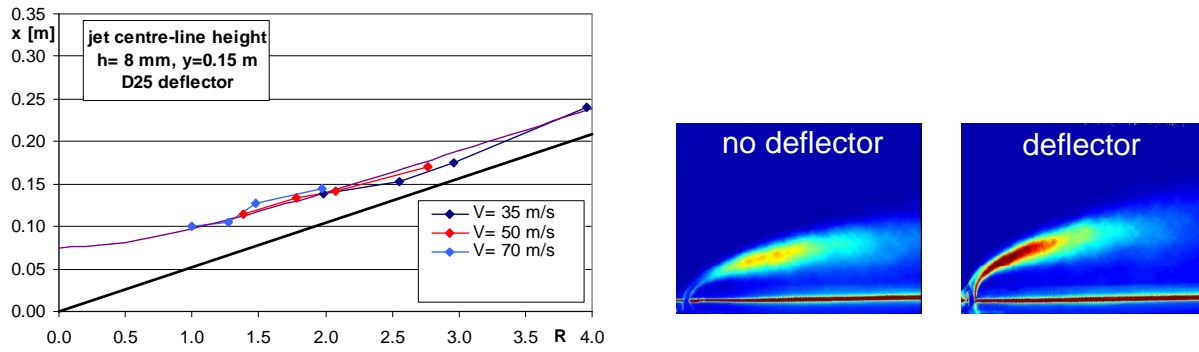


Figure 22: Jet centerline height as a function of velocity ratio  $R$  at a streamwise distance of  $y = 0.15$ , for the 8-mm normal blowing slot with 25-mm quarter-circle deflector. The straight black line shows the relationship without deflector (Eq. (2.2) with  $c_j = 1.5$ ). The curved purple line shows the relationship according to Eq. (2.6), with  $c_v = 0.3$ .

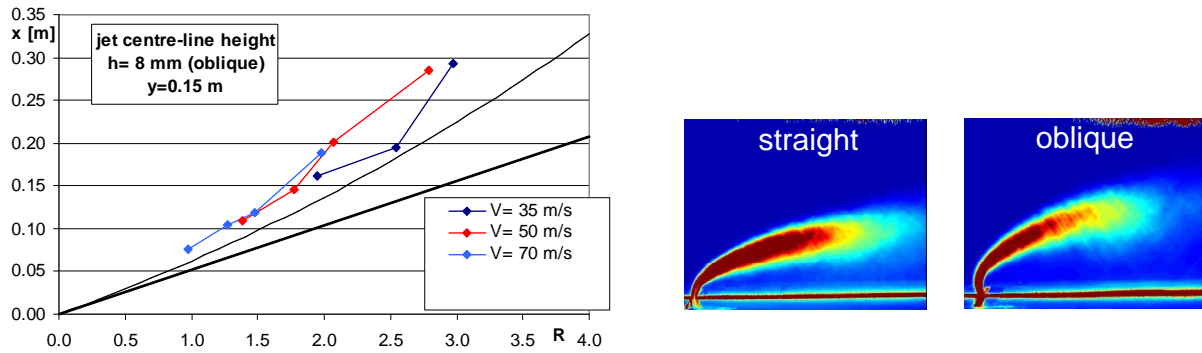


Figure 23: Jet centerline height as a function of velocity ratio  $R$  at a streamwise distance of  $y = 0.15$ , for the 8-mm oblique blowing slot. The straight black line shows the relationship for normal blowing (Eq. (2.2) with  $c_j = 1.5$ ). The curved black line shows the relationship according to Eq. (2.8), with  $c_v = 0.3$ .

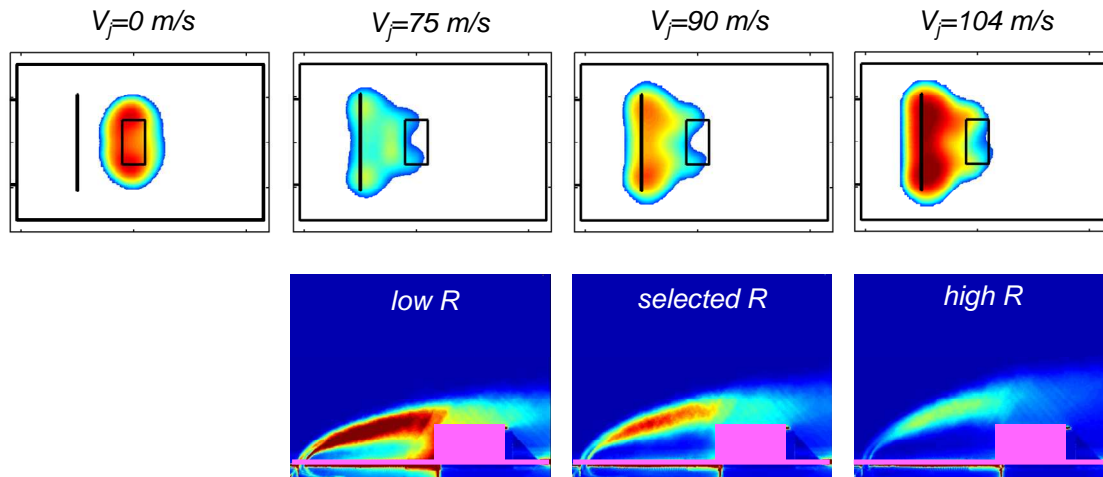
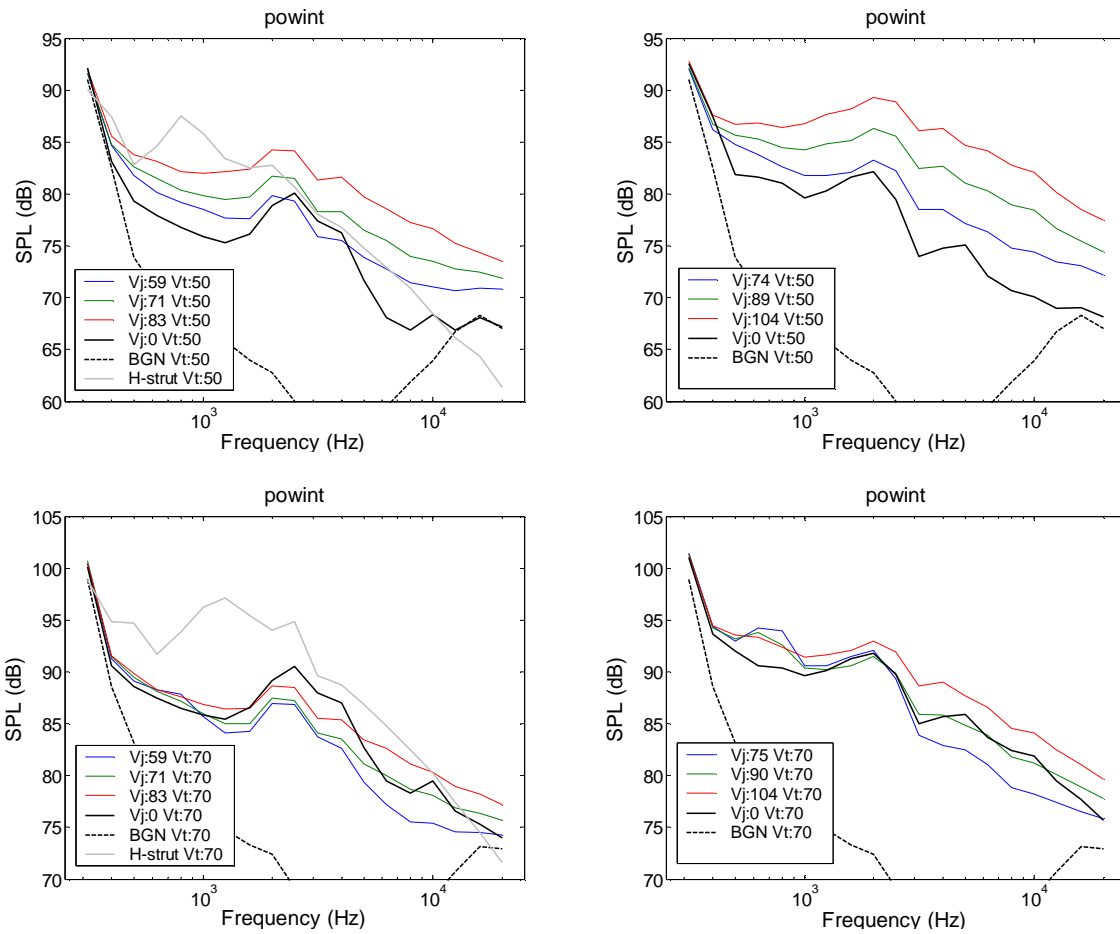
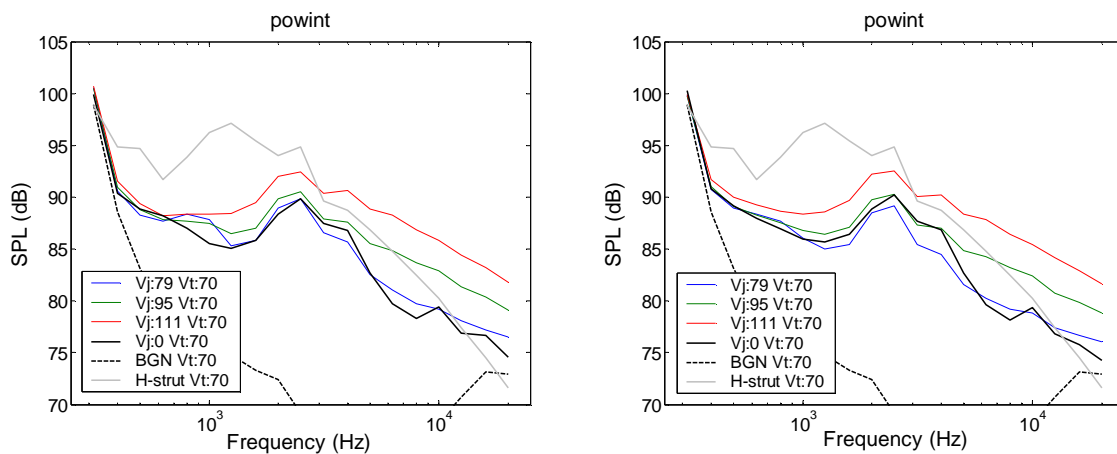


Figure 24: Acoustic source maps (4 kHz) and average PIV plots for 50-mm model behind the 11-mm normal blowing slot, at different blowing speeds ( $V = 70$  m/s).



**Figure 25: Integrated spectra for 25-mm (left) and 50-mm (right) models with and without 11-mm normal air curtain, for downstream model position at V= 50 (top) and 70 m/s (bottom).**



**Figure 26: Integrated spectra for 25-mm model with and without 8-mm normal air curtain at V= 70 m/s, for upstream (left) and downstream (right) model positions.**

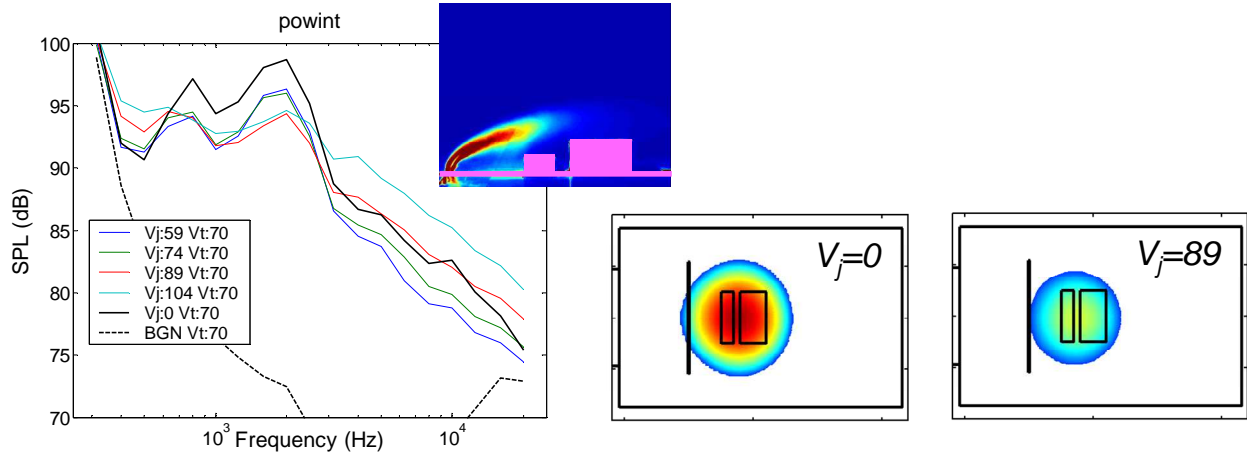


Figure 27: Integrated spectra and source maps (1.6 kHz) for combined model with and without 11-mm normal air curtain at  $V=70$  m/s.

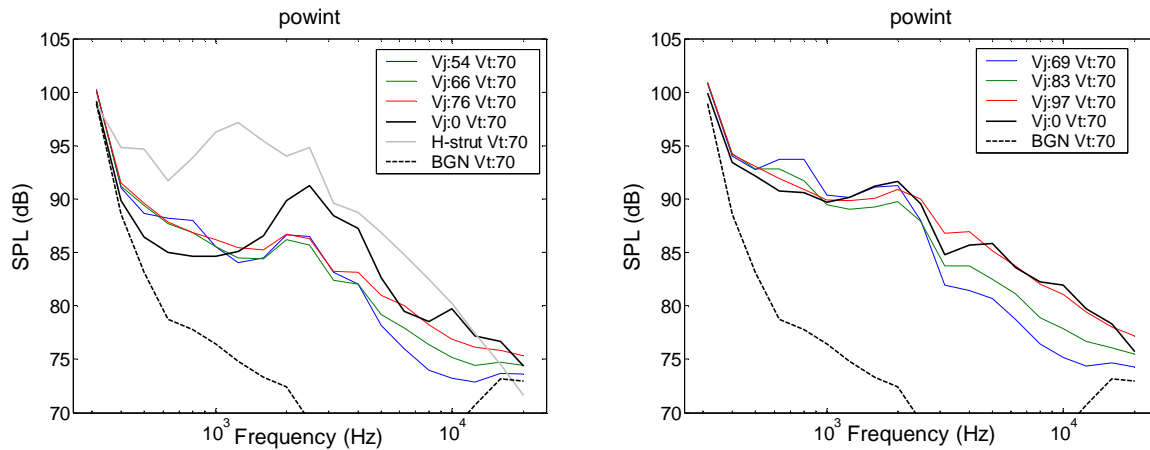


Figure 28: Integrated spectra for 25-mm (left) and 50-mm (right) models with and without 8-mm oblique air curtain, for downstream model position at  $V=70$  m/s.

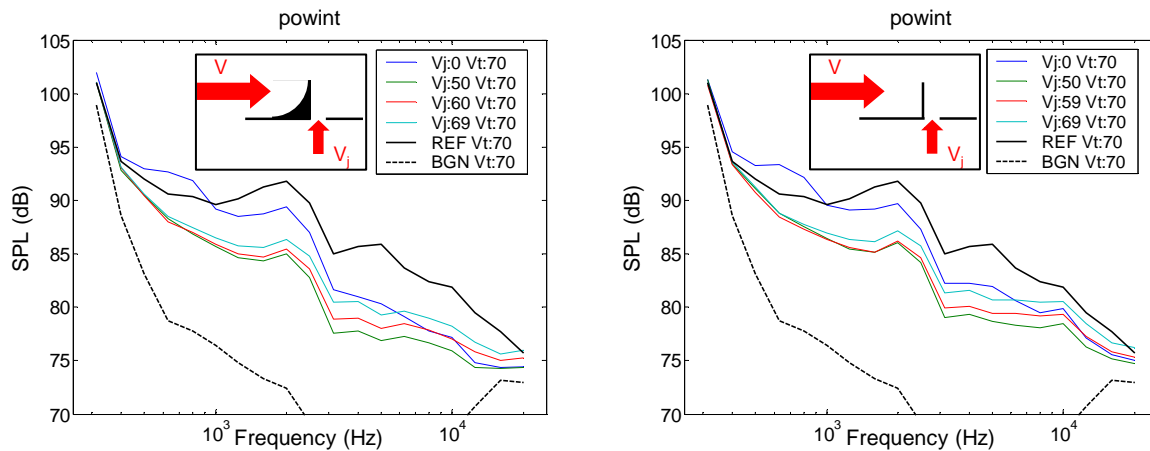


Figure 29: Integrated spectra for 50-mm model with and without 11-mm normal air curtain with 25-mm quarter-circle deflector (left) and 25-mm rectangular deflector (right), for downstream model position at  $V=70$  m/s. 'REF' indicates the baseline model noise without deflector.